Popular Summary

Convective - Stratiform Precipitation Variability at Seasonal Scale from Eight Years of TRMM Observations: Implications for Multiple Modes of Diurnal Variability

Song Yang and Eric A. Smith

Atmospheric convective systems (such as storms and tornados) and stratiform systems (such as anvil clouds, clouds following a passing front) have important impacts on economy, human activities and modern society. More knowledge of the convective and stratiform activities will be helpful for computer models used to improve weather predictions. The precipitation radar onboard the satellite of the first joint Tropical Rainfall Measuring Mission (TRMM) by the US National Aeronautics and Space Administration (NASA) and Japan Aerospace Exploration Agency (JAXA) launched on November 22, 1997 provides a unique long-term dataset of convective and stratiform rainfall over the global tropics. This study uses 8-year TRMM convective and stratiform rainfall to display spatial patterns and seasonal changes. These features are useful for computer modelers to evaluate their models performance. Results show that the total rainfall over oceans has a major diurnal peak in late evening – early morning and a minor diurnal peak in afternoon, while the continental rainfall has opposite diurnal phases. This study gives evidence of the major diurnal peak controlled by convective rainfall and the minor diurnal peak controlled by the stratiform rainfall. In addition, the rainfall diurnal modes are largely due to the rainfall diurnal stratiform variations modulating the convective variations. Results demonstrate the importance of stratiform rainfall diurnal variability.

Convective - Stratiform Precipitation Variability at Seasonal Scale from Eight Years of TRMM Observations: Implications for Multiple Modes of Diurnal Variability

Song Yang [1] and Eric A. Smith [2]

[1] Center for Earth Observing and Space Research, College of Science, George Mason University
Fairfax, VA; MailStop -- NASA/GSFC, Laboratory for Atmospheres (Code 613.1)
Greenbelt, MD 20771, USA [301-614-6338 ; ysong@agnes.gsfc.nasa.gov]

[2] NASA/Goddard Space Flight Center, Laboratory for Atmospheres (Code 613.1)
Greenbelt, MD 20771, USA [301-614-6286 ; eric.a.smith@nasa.gov]

June 2007

Submitted to Special Issue in
AMS Journal of Climate
"*Understanding Diurnal Variability of Precipitation through Observations and Models*"

Corresponding Author

Dr. Song Yang
NASA/Goddard Space Flight Center
Laboratory for Atmospheres (Code 613.1)
Greenbelt, MD 20771, USA
Email: ysong@agnes.gsfc.nasa.gov

Abstract

This study investigates the variability of convective and stratiform rainfall from eight years (1998-2005) of Tropical Rainfall Measuring Mission (TRMM) Precipitation Radar (PR) and TRMM Microwave Imager (TMI) measurements--focusing on seasonal diurnal variability. The main scientific goals are: (1) to understand the climatological variability of these two dominant forms of precipitation across the four cardinal seasons and over continents and oceans separately, and (2) to understand how differences in convective and stratiform rainfall variations ultimately determine how diurnal variability of total rainfall is modulated into multiple modes.

There are distinct day-night differences for both convective and stratiform rainfall. Oceanic (continental) convective rainfall is up to 25% (50%) greater during nighttime (daytime) than daytime (nighttime). Seasonal variability of convective rainfall's day-night difference is relatively small, while stratiform rainfall exhibits very apparent day-night variations with a seasonal variability of these variations. There are consistent late evening diurnal peaks without obvious seasonal variations over ocean for convective, stratiform, and total rainfall. Over continents, convective and total rainfall exhibit a consistent dominant afternoon peak with little seasonal variability--with a late evening secondary peak exhibiting seasonal variation. Stratiform rainfall over continents shows a consistent strong late evening peak with a weak afternoon peak--with the afternoon mode undergoing seasonal variability. Therefore, the diurnal characteristics of stratiform rainfall control the afternoon secondary maximum of oceanic rainfall and the late evening secondary peak of continental rainfall. Even at seasonal-regional scale spatially or an interannual global scale temporally, the secondary mode can become very pronounced, but on an intermittent basis. Overall, the results demonstrate the importance of partitioning total rainfall into convective and stratiform components and that diurnal modes largely arise from distinct diurnal stratiform variations modulating convective variations.

1. Introduction

Understanding space-time variations of precipitation is an important topic in climate research, in which modern, high quality, global-scale precipitation observations are essential. Detailed analyses of such datasets reveal the evolution and lifetime of precipitating clouds, including the embedded convection and stratiform forms of precipitation, all of which help improve rainfall climate predictions. High quality, global scale coverage of precipitation first became available with satellite-derived passive microwave (PMW) measurements obtained from Defense Meteorological Satellite Program (DMSP) satellites flying the Special Sensor Microwave Imager (SSM/I), first flown in July 1987. These were important new measurements because they were acquired consistently for both continental and oceanic environments (Smith et al. 1998). One of the first satellite rainfall programs to then produce a long-term global record of rainfall from satellite measurements was the Global Precipitation Climate Project (GPCP), whose principal objective has been to support climate research and hydrological applications (Huffman et al. 1997). For example, large-scale distributions of precipitation have been applied in climate diagnostic studies (Rasmusson and Arkin 1993), validation of rainfall forecasts from numerical weather prediction models (Janowiak 1992), and as input for surface process models (Shinoda and Lukas 1995). Also, rainrates derived from globally-distributed satellite data used for input to numerical prediction models have resulted in improved forecast skill and storm predictions (Krishnamurti et al. 2001; Hou et al. 2004).

Notably, newer satellite measurements from instruments flown on the Tropical Rainfall Measuring Mission (TRMM) satellite, i.e., the 9-channel TRMM Microwave Imager (TMI) PMW radiometer and the Ku-band (13.8 GHz) Precipitation Radar (PR) developed by the U.S. and Japanese space agencies [National Aeronautics and Space Administration (NASA) and Japan Aerospace Exploration Agency (JAXA)] (Simpson et al. 1996), the NASA/JAXA

Advanced Microwave Scanning Radiometer (AMSR) flown on NASA's AQUA satellite (a 12-channel total-power radiometer using 6 frequencies from 6.9 to 89 GHz, and the NASA/Canadian Space Agency (CSA) W-band (94 GHz) Cloud Profiling Radar (CPR) flown on the NASA CloudSat satellite (L'Ecuyer and Stephens 2002; Stephens et al. 2002) have enabled much more advanced global-scale precipitation analysis. Motivated by these advances, the goal of this study is to extend our understanding of global precipitation characteristics through analysis of the seasonal variability of convective and stratiform rainfall based on the use of long-term records of TRMM rainfall (8 years over 1998-2005 period) obtained from PR and TMI measurements -- over the tropical global province.

Overall, the principal scientific objectives of this study are: (1) to understand the climatological variability of convective and stratiform precipitation on a seasonal basis, classified by continental and oceanic environments, and (2) to understand how differences in convective and stratiform rainfall variations modulate the diurnal variability of total rainfall into multiple modes. Our most important findings are that: (1) there is a dominant diurnal mode resulting from either a pure or partial convective primary harmonic, which differentiates between continents and ocean, and (2) there is a secondary mode representing either a weak or strong stratiform harmonic, which serves to modulate the convective mode -- but with strong dependence on environmental background, season, region, and the specific annual period.

The most physical approaches for retrieving rainfall and its associated latent heating impacts, particularly over oceans, are associated with microwave algorithms, either passive or active or both (Meneghini and Kozu 1990; Iguchi and Meneghini 1994; Wilheit et al. 1994; Haddad et al. 1997, 2004; Smith et al. 1997, 1998; Ebert and Manton 1998; Yang and Smith 1999a-b, 2000; Iguchi et al. 2000; Kummerow et al. 2000, 2001; Meneghini et al. 2000, Tao et al. 2006). The TRMM satellite was the first dedicated to retrieval of rainfall measurements and thus was able to

justify the use of the purely physical methodologies (Simpson et al. 1988, 1996). The TRMM project produces accurate precipitation estimates from two instruments designed specifically for measurement of rain rate according to Ku-band radar reflectivity and multi-frequency passive microwave attenuation and scattering (Kummerow et al. 1998). To date, TRMM has provided reliable, continuous, and accurate rain rate estimates based on various physical algorithms over the global tropics and sub-tropics that have led to greater understanding of precipitation processes and variability (Kummerow et al. 2000; Wolff et al. 2005; Yang and Smith 2006; Yang et al. 2006a-b; Smith et al. this issue; Yang et al. this issue).

Precipitation classified into convective and stratiform categories is an important scientific distinction, recognizing that this capability has only been made possible by the availability of PR space radar measurements whose detailed vertical reflectivity structures reveal distinct profile slope properties that are closely associated with either convective or stratiform environments (Haddad et al. 1997; Iguchi et al. 2000). Another important phenomenon vis-à-vis precipitation processes is diurnal variability (Yang and Smith 2006). With the availability of high quality, global scale, and long-term rainfall datasets from satellite observations, the study of the diurnal cycle of rainfall has been renewed. This topic was first examined as a scientific phenomena over 100 years ago (Hann 1901), and has been studied extensively since that time in intermittent periods. Yang and Smith's (2006) study of diurnal mechanisms based on TRMM data includes a detailed review of the 20th century literature.

In the last decade, there have been a few studies focused on understanding the relative amounts of convective and stratiform rainfall at lower latitudes. Required reading is the paper of Houze (1997) who drew attention to the somewhat paradoxical idea of even referring to stratiform rainfall in the tropics, given that for so many decades, meteorologists had restricted their physical definition of this rainfall category such that stratiform precipitation was taken as a

strictly midlatitude, cold-rain phenomenon occurring only in baroclinic cyclones. It was the Houze (1997) paper that emphasized the fact that in the tropics, there is no separating convective and stratiform rainfall, because, in essence, stratiform rainfall at lower latitudes represents convection at the end of its precipitating life cycle -- or more prosaically, "old convection". Moreover, stratiform rainfall also occurs in the tropics as a warm rain process. This can be troublesome when trying to classify precipitation based on the occurrence of a sharp radar "bright band" feature in the reflectivity profile that generally denotes the stratiform phase of a cold rain precipitation life cycle in which large frozen hydrometeors (e.g., snowflakes, aggregates, graupel, and/or hail) fall through the melting level and begin taking on the characteristics of excessively large liquid rain drops, insofar as a radar is concerned.

The study by Steiner et al. (1995) demonstrated how a combination of rain gauge and Doppler ground radar data could be used to classify precipitation into convective and stratiform categories. A partly similar study was conducted by Geerts and Dawei (2004) based on vertical pointing airborne radar measurements of reflectivity and line-of-sight Doppler velocity. There has even been an attempt by Tremblay (2005) to classify precipitation into its convective and stratiform components based on fitting exponential functions to only surface rain gauge measurements. A much more robust study involving the use of TRMM's PR space radar, Schumacher and Houze (2003) reported that over the tropics, stratiform rainfall accounts for ~73% of the area covered by rain while yielding some 40% of the total rainfall accumulation. In addition, they noted that convective rainrates were, on average, some 4 times stronger than stratiform rainrates -- all of which indicates that stratiform rainfall is a very important tropical precipitation mode with rather complex physical properties.

Although there are many proposed mechanisms to explain the diurnal cycle of precipitation, it is generally accepted that a widespread afternoon rainfall peak over continents is due to a post-

noon maximum in surface heating and the resultant static instability. However, over oceans, there are a number of mechanisms that have been proposed to explain the endemic late evening-early morning rainfall maximum. In our view, three of these have obtained conspicuous traction. The first can be called the "static radiation-convection" (SRC) interaction. This is a synoptic scale mechanism which presumes that enhanced cloud-top IR cooling at night, stemming from the lack of cloud-top solar absorption, and a consequent increase in the thermal lapse rate (Kraus 1963, Lavoie 1963, Ramage 1971), leads to stronger convection and nighttime rainfall. The SRC mechanism enables radiative forcing to favor more intense rainfall during the late night period, provided a pre-existence of cloudiness.

The problems with this mechanism in explaining diurnal variability in deep convective environments stems from the fact that significant differences between daytime-nighttime oceanic lapse rates are not observed (Betts 1982, Emanuel 1986, 1994, Xu and Emanuel 1989). Moreover, the troposphere may actually become stabilized from deep cumulus layer overturning (Ruprecht and Gray 1976, Gray and Jacobson 1977). However, SRC is the favored mechanism found in a study by Randall et al. (1991) based on a general circulation model (GCM). Lin et al. (2000) reported that diurnal phasing in the Randall GCM is very sensitive to a specified parameter which links cumulus kinetic energy to cloud mass flux – thus rendering the initial study open to question concerning model validity.

The second oceanic mechanism of interest can be called the "dynamic radiation-convection" (DRC) interaction, based on the assumption that day-night differences persist in radiative cooling over deep convection in contrast with the surrounding clear-air areas. This effectively suppresses daytime convection, leading to more nighttime rainfall. Daytime suppression results from clear regions experiencing less subsidence warming in response to ongoing radiative cooling because of enhanced daytime radiative heating due to water vapor, thus reducing

convergence into the convection zone and inhibiting daytime convective growth. Ruprecht and Gray (1976) and Gray and Jacobson (1977) first proposed this mechanism, later supported by Foltz and Gray (1979), McBride and Gray (1980), and Ackerman and Cox (1981). However, it is only applicable to extended organized convection (e.g., meso-α scale mesoscale convective systems, tropical cyclones, and synoptic scale convergence zones) where background subsidence can be altered at regional scales.

Notably, regardless that both SRC and DRC diurnal interactions are rooted in daytime-nighttime radiative cooling differences, the two mechanisms are diametrically opposed in explaining which portion of the diurnal cycle is actually perturbed by the underlying forcing mechanism. The SRC interaction favors nighttime enhancement through increased thermodynamic instability, while the DRC interaction favors daytime suppression through decreased daytime convergence into the convection zone.

The third oceanic mechanism of note draws attention to two control factors which can effect the timing of diurnal precipitation variability, specifically, the ambient precipitable water (PW) and the cloud-storm life cycle that microphysically evolves over time to produce precipitation. Based on TOGA-COARE data and numerical modeling experiments, Sui et al. (1997, 1998) found that the nocturnal precipitation mode can be explained by relatively more available condensed moisture available at night due to diurnally varying radiative cooling, with the resultant change in tropospheric moisture stimulating condensation and precipitation. This mechanism, referred to as SRCM and also addressed in the modeling studies of Tao et al. (1993, 1996), is in contrast with the Randall et al. (1991) SRC explanation that the key diurnal control is simply nighttime thermodynamic destabilization of lapse rates.

Yang and Smith's (2006) recent review and TRMM data analysis concerning mechanisms of diurnal rainfall variability found that the earlier published mechanisms were mostly based on

limited regional datasets that lacked context and duration, and thus could not reveal all of the key processes which produce the endemic complexity inherent to the diurnal cycle of precipitation when examined in detail and over extended space and time scales. Using one year of high resolution, level 2 TRMM rainfall retrieval products, they found that diurnal rainfall variability is a richly textured global phenomenon with embedded diurnal harmonics which produce complexities that generally cannot be explained by individual causal factors. For example, on a seasonal-regional basis, the primary late evening/early morning oceanic rainfall maximum is often accompanied by a secondary afternoon peak. Conversely, the dominant mid- to late-afternoon continental rainfall maximum is often replaced or accompanied by a secondary morning peak. In fact, the main underlying lesson from their TRMM analysis is that there are a host of mechanisms at work producing diurnal rainfall variability, no single one of which can explain *the* entire process or in general, *an* entire process. Instead, a mixture of two or more mechanisms (modes) are generally at work over regional and smaller scales, combining together to produce the averaged process at larger scales. Thus, the trick in understanding diurnal rainfall variability is to understand the contexts and modal components producing the averaged effects (that quite often become blurred through the imposed averaging), and then diagnosing the appropriate physical mechanism(s) underlying the processes being averaged.

This is why we are investigating the diurnal variability of the separate convective and stratiform components contributing to the overall diurnal variability of total rainfall. We will show that this is very important in interpreting the multi-modal nature of diurnal rainfall behavior. Although there is a history of literature that has investigated the spatial structures and temporal variations of convective and stratiform precipitating cloud systems (Houze 1989; Short et al. 1996; Schumacher et al. 2004), almost no research has explored differences in their individual diurnal properties. Since the tropics experience the greatest precipitation loading, the

long term, global-scale, diurnally-sampled TRMM rainfall products are ideal for studying spatiotemporal variations of partitioned convective and stratiform precipitation.

Results from this study are intended to improve our understanding of the mean and variable horizontal distributions of convective and stratiform rainfall, with the more important goal of explaining how distinct convective-stratiform precipitation properties determine the diurnal behavior of total rainfall in a multi-modal framework. Finally, the similarities and differences of retrieved convective and stratiform rainfall from different TRMM algorithms will help guide the improvement of these and other algorithms for the next-generation Global Precipitation Measurement (GPM) Mission (Smith et al. 2007).

2.0 Methodology and Datasets

Due to the nature of the TRMM satellite design, sampling error is always an issue when a small time scale is considered for studying rainfall diurnal variations (Negri et al. 2002; Hirose and Nakamura 2005). Yang and Smith (2006) and Yang et el. (2006a) have shown for the mean rainfall diurnal cycle, the sampling issue is abated when a seasonal scale is considered.

2.1 Methodology

Convective and stratiform separation is obtained from TRMM PR rain classification algorithm 2a23. Raining pixels are categorized into three different rain types: (1) convective, (2) stratiform, and (3) "other". The classifications are based on the combination of a vertical profile method (V-method) and horizontal profile method (H-method) described by Awaka et al. (1997, 2007). The V-method can be summarized in three steps: (1) a raining pixel is classified as stratiform when a bright band (BB) exists; (2) a raining pixel is classified as convective when the maximum reflectivity (Z) is greater than 39 dBZ without existence of the BB; and (3) all other raining pixels are defined as "other". The H-method is based on a convective/stratiform separation scheme in which the horizontal pattern of Z at a given height is examined (Steiner et

al. 1995). A raining pixel is convective when Z exceeds a Z_{max} threshold of 40 dBZ or Z stands out against the background area. For this situation, the nearest four pixels to the assigned convective pixel are also defined as convective. Then, the other surrounding raining pixels are defined as stratiform. Pixels are classified as "other" when the radar echo below the freezing level (less a 1 km margin) is very weak so that "other" rain pixels defined by the H-method indicate either cloud or noise. The V-method and H-method are first applied separately, then their unified result is used to classify the raining pixel into one of the three categories. The use of these definitions ensures that rainfall amount derived from "other" rain pixels is very small. A detailed description of this rain type classification procedure is found in TRMM Science Data and Information System (TSDIS) file specifications under dataset 2a23 (see TSDIS 2006).

The categorized rainfall over a 0.5°x0.5° latitude-longitude grid from different TRMM rain algorithms for a season are initially accumulated. Three-hour rainfall compositing is also applied in analyzing rainfall diurnal variations. These averages are then further regrouped depending on different temporal-spatial scales used for a specific analysis. Also, five oceanic and one continental region, all with climatologically active rainfall regimes, are selected to illustrate the regional variations of convective and stratiform rainfall.

2.2 Description of Datasets

Eight years (1998-2005) of Version-6 (v6) TRMM rain products are taken from three standard level 2 algorithms -- 2a12, 2a25, and 2b31. The 2a12 algorithm consists of a TMI-only microphysical profile scheme cast in Bayesian form, which uses a cloud resolving model (CRM) to generate numerous microphysical profiles of various liquid and frozen hydrometeors for rainfall (R) conditions as a solution-basis, in which solutions arise by combining microphysical profiles into weighted averages determined from the proximity of pre-calculated forward radiative transfer calculations associated with the individual microphysical profiles to the TMI's

channel-specific measurement values (Kummerow et al. 1998; Olson et al. 2006). The 2a25 algorithm consists of the PR-only rainrate profile scheme, akin to the top-down Hitschfeld-Bordan recursive scheme, that uses a PR-based climatology of cloud-free surface radar cross-section (σ_r) to re-assign total path attenuation (A) and a pre-specified Z-R relationship for defining allowable rain microphysics. The coefficients of the initial unified Z-R/Z-A relationships, designed to yield top-down attenuation path during a 1st pass, are adjusted in a 2nd pass so that the final R profile gives rise to the A estimated from the surface reflectance method (Iguchi and Meneghini 1994; Meneghini et al. 2000). The 2b31 algorithm consists of a combined PR-TMI rainrate profile scheme, based on what has been referred to as a combined "tall vector" solution. The "tall vector" solution is also cast in Bayesian form, with all Zs from the PR-measured rain gate vectors and radiometer-measured brightness temperatures (TBs) from the TMI-measured channel vectors used in an "instrument-balanced" concatenated inversion scheme. The microphysical database is drawn from both disdrometer observations (from Darwin, Australia and the TOGA-COARE field experiment) and CRM-generated microphysics (Haddad et al. 1997; Smith et al. 1997). This process is guided by three Bayesian sweeps for calculating total path attenuation, i.e., (1) an initial top-down Hitschfeld-Bordan pass, (2) a 2nd climatologically-derived σ_r-based pass, and (3) a final 10.7/19/37 GHz TMI measurement-based pass. The beam discrepancy between the PR and TMI instruments is resolved through a deconvolution procedure with retrieved rainrate values taken at native PR spatial resolution.

3.0 Characteristics of Seasonal Convective and Stratiform Rainfall

The 8-year (1998-2005) mean monthly surface rainfall fields from the 2a12, 2a25, and 2b31 algorithms are illustrated in Figure 1. The horizontal distributions are highly consistent with each other exhibiting well-known climatological precipitation characteristics such as heavy

rainfall within the inter-tropical convergence zone (ITCZ), the southern Pacific convergence zone (SPCZ), the Asian Monsoon region, the African and South American tropical rainforests, and the subtropical storm tracks including the feature over and off southern Brazil's east coast.

Since different physical assumptions are used in the three retrieval algorithms, differences amongst them should be expected. The slightly larger rainfall of 2a12 and slightly smaller rainfall of 2a25 are apparent in Fig. 1. These small discrepancies in the global mean magnitudes are consistent with comparison results found at different space-time scales by Wolff et al. (2005), Yang and Smith (2006), and Yang et al. (2006a-b). However, the most salient feature of the three rainfall distribution is their overall similarity in terms of the pattern of the distributions. The near agreement in the means and the almost exact pattern agreement affirm that the three level-2 based v6 TRMM rainfall time series reveal a highly consistent near-decadal climatology of precipitation over the global tropics and subtropics.

Using 3-month compositing, Figure 2 shows the horizontal distributions of 8-year mean rainfall from the 2b31 combined algorithm for the four cardinal seasons. [Very similar patterns of seasonal rainfall are found in the 2a12 and 2a25 rainfall products -- not shown.] It is evident that the Spring precipitation distribution has a dominant maximum over the equatorial area of the west Pacific Ocean and east Indian Ocean, but relatively weak ITCZ rainfall. In Summer, maximum rainfall is found over the Bay of Bengal, with rainfall over the Indian and Indonesian regions acting as an integral part of the Asia Summer Monsoon's major convection sources. The large amplitude of rainfall over the tropical east Pacific Ocean and across the northwest South American coastal zone is also associated with storm-generated convection. The local maxima of rainfall over the tropical east Atlantic Ocean and over Africa are likely due to convection produced within tropical easterly waves. Also, there is obvious intensification of ITCZ rainfall during Summer in relationship to ITCZ activity during Spring. The Autumn rainfall distribution

exhibits a maximum over the equatorial areas of the east Indian Ocean and west Pacific Ocean warm pool regions. In Winter, the rainfall pattern is highly contrasted relative to Summer. The dominant feature is the large belt of activity along the equatorial zone with maxima over the west Pacific and east Indian Oceans and the ITZ-SPCZ intersection in the west Pacific referred to as the "V" sector. Weak rainfall over the Asian Monsoon region is evident. The relative increase of rainfall over the north Pacific Ocean is linked to winter midlatitude frontal systems.

Figure 3 presents 8-year mean seasonal zonal rainfall from the three algorithms over ocean and continent. It is apparent that the zonal distributions with respect to the algorithms exhibit similar features, in which the oceanic profiles are nearly identical -- perhaps with the exception of Winter in which there are slight discrepancies within a few confined latitude bands. The discrepancies are larger over the continents in which 2a12 exhibits consistently larger tropical and Northern Hemisphere subtropical amplitudes. For oceanic rainfall, the zonal profiles for Summer and Autumn are similar, with a dominant peak near 7.5°N caused by the seasonal northward migration of the ITCZ. The Winter and Spring oceanic profiles also exhibit similar features with a main peak near 5°N and a secondary peak near 7.5°S. The southward ITCZ movement along with the intensification of the SPCZ during the Austral Summer and Autumn periods lead to this double peak structure. In the case of continental rainfall, the maximum amplitudes are located in the Northern Hemisphere (NH) during Spring and Summer (mainly due to the Asian Monsoon), shifting to the Southern Hemisphere (SH) during Autumn and Winter partly due to the onsets of the rainy seasons in South Africa and South America. The unrealistically large rainfall features exhibited by 2a12 north of 20°N during Winter and Spring draw attention to the fact that rainfall retrieval over cold land surfaces remains an unresolved problem for radiometer-only algorithms. However, the v6 TRMM rain products exhibit

significant improvement compared to the earlier v4 and v5 releases; see Kummerow et al. (2001), Olson et al. (2006), Yang et al. (2006b).

A similar analysis is then conducted for algorithms 2a25 and 2b31, but now including partitioning into convective and stratiform rainfall categories, with results shown in Figure 4. [It can be seen that, in general, the two algorithms exhibit nearly identical results.] More importantly, the distribution patterns of zonal mean convective and stratiform rainfall are similar, including similar magnitudes. The fact that these distribution patterns are close to the total rainfall pattern, shown in Fig. 3 over the higher amplitude latitude bands, simply denotes that convective and stratiform rainfall are nearly equal in importance in contributing to total precipitation over the global tropics. For the oceanic regime, there is relatively more convective than stratiform rainfall over the heavy rainfall latitudes including those of the ITCZ, SPCZ, Asia Summer Monsoon, and African wet season. In contrast, there is much more stratiform rainfall over the smaller amplitude subtropics due to the greater role of frontal rainfall stemming from tropical-midlatitude interactions. As with oceanic rainfall, there are relatively greater convective amounts over the continental heavy rainfall latitude zones, but in contrast to the oceanic regime, seemingly nearly equal contributions in the subtropics.

To emphasize the contrasts, relative contributions (given in percent) to total seasonal rainfall from the convective and stratiform categories are shown in Figure 5. [As in Fig. 4, the results are nearly identical with respect to the two algorithms.] Now the actual differences, in terms of contribution between the tropics and subtropics and between the oceanic and continental regimes, are obvious. For ocean, the contributions by the two categories in the tropics are nearly equal (~50% each), whereas there is a much greater contribution by stratiform rainfall in the subtropics (ranging up to 80%). Over continents, in Summer and Autumn, some 60% of rainfall is due to convective rainfall over the heavy rainfall latitudes, while there are much greater

stratiform contributions in the subtropics during SH Summer and NH Autumn -- where precipitation is relatively weak as noted in the results shown in Fig. 4. The cross-season dissimilarities over the continents are found in the heavy rainfall portions of the SH Winter and Spring tropics where convective-stratiform contributions are nearly equal (~50%), with contributions by convective rainfall ranging up to 70% over the equatorial zone and into the NH northern edge of the high amplitude rainfall zone. In both Winter and Spring in the NH subtropics, contributions due to stratiform rainfall significantly exceed those due to convective rainfall -- but conversely, the contribution due to convective rainfall in the SH subtropics during Winter dominates (this same feature appears in the NH Summer subtropics to a lesser degree). This feature of continental convective and stratiform rainfall partition in subtropics during Summer and Winter is similar to the convective and stratiform separation based on the 2001 surface rain gauge measurements (Tremblay, 2005). This feature is possibly associated with the interannually progression of the ITCZ and more frontal rainfall contributions in the subtropics of the Winter hemisphere.

Figure 6 presents horizontal distributions of seasonal convective and stratiform rainfall contributions to total rainfall from the 8-year 2a25 dataset. [Similar patterns are found in the 2b31 dataset.] These results show that, in general, the percentage of convective rainfall over continents exceeds 50%, except over most of East Asia and Australia where convective rainfall contributions drop to 20%. Also, the contribution due to convective rainfall over North America is less than 50% during Autumn and Winter, also falling below 50% in Central America and South America during the boreal Winter and Spring because of the tendency for cold-season frontal band stratiform rainfall. Over the maritime domain, contributions by convective rainfall over the Atlantic and Indian Oceans generally exceed 50%. These contributions range up to 70% over the western tropical area of the south Pacific Ocean and the entire tropical area of the south

Atlantic Ocean where rainfall is mostly weak, emanating often from shallow cumulus convection (Short and Nakamura, 2000). Over portions of the SPCZ, the convective rainfall contribution is actually less than 50%, especially over its southern segment. Alternatively, convective rainfall within the Pacific Ocean's ITCZ generally exceeds 50% of the total -- except over the west Pacific equatorial band during Spring and Summer and the east Pacific ITCZ during Autumn.

The results in Fig. 6 draw attention to the obvious seasonal and regional variabilities found in the relative contributions by convective and stratiform rainfall. Summary results of the horizontal distribution analysis from both the 2a25 and 2b31 datasets are given in Table 1. [Here, it is evident that the rainfall contributions from the "other" rainfall category are very small.] Over ocean, seasonal variations of convective or stratiform rainfall contributions are small (~ 2%) for both algorithms. The overall percentages of oceanic convective (stratiform) rainfall are ~45% (~55%) for 2a25 and ~42% (~58%) for 2b31 -- within the expected range of uncertainty between algorithms. The continental convective and stratiform rainfall contributions exhibit large seasonal variations up to 8% for 2a25 and 11% for 2b31. The overall percentages of continental convective (stratiform) rainfall are ~52% (~48%) for both 2a25 and 2b31.

Our results are comparable with earlier results reported by Tao et al. (2000) over selected regions based on their use of a limited 2a12 dataset. Rutledge and Houze (1987), Johnson and Hamilton (1988), and Houze (1997) have found that stratiform rainfall is typically about 40-50% for oceanic convective systems in the tropics, but smaller (about 30-40%) for continental convective systems. Note, these values of stratiform rainfall contribution are less than our long term mean values over the global tropics, but in line with our findings over selected regions.

4.0 Seasonal Variability of Convective and Stratiform Rainfall

Yang and Smith (2006) have described day and night differences of precipitation based on a one-year TRMM dataset. On average, they found that there is relatively more nighttime rainfall

than daytime rainfall over oceans, and more daytime rainfall than nighttime rainfall over continents. In this study, the eight year TRMM data have been analyzed to remove any possible biases due to interannual variability that may have affected the Yang and Smith (2006) study.

4.1 Day - Night Variations

Figure 7 shows seasonal variations of spatial ratio distributions of daytime to nighttime rainfall from the 8-year 2a25 and 2b31 datasets. The highly coherent ratio distributions demonstrate that the underlying rainfall features are robust. The overall contribution due to daytime oceanic rainfall is generally as much as 25% lower than the contribution due to nighttime rainfall, while continental daytime rainfall is generally up to 25% greater than nighttime rainfall. The overall seasonal variation of daytime to nighttime rainfall ratio is not very significant. However, seasonal variations of day to night rainfall ratio are obvious at regional scales, such as over eastern China, the United States and Gulf of Mexico area, the west coast area of Australia, the Arabian Peninsula region, and the north Pacific Ocean.

Notably, the marine stratocumulus (MSC) areas show more detailed day to night rainfall variations than were discussed by Yang and Smith (2006). Daytime rainfall exceeds nighttime rainfall over the North/Central American MSC region in Spring, Summer, and Winter, with opposite behavior in Autumn. However, there is generally more nighttime rainfall over the South American MSC region. The west African MSC region exhibits more daytime rainfall in Winter and Spring, with opposite behavior in Summer and Autumn. More rainfall during daytime is also found in the South Africa MSC area in Spring and Autumn, with opposite behavior in Summer and Winter. The eastern Arabian Sea MSC area clearly exhibits more daytime rainfall, except during Winter. The general propensity of MSC rainfall to exhibit a daytime maximum is important because it suggests that a controversial daytime convective overturning mode dominates over a generally accepted nighttime stratiform drizzle mode.

Figure 8 presents the spatial ratio distributions of daytime to nighttime convective and stratiform rainfall. The distribution patterns for convective rainfall are somewhat similar to those of total rainfall, except the continental convective rainfall contributes as much as 50% more rainfall in daytime than in nighttime. These results elucidate how in the mean, convective rainfall dominates during daytime over continental regions and surrounding areas, while over oceans, it dominates during nighttime, helping corroborate by use of a lengthy TRMM dataset, earlier reported results (e.g., Hann 1901; Gray and Jacobson 1977; Dai 2001; Yang and Smith 2006; Yang et al. 2006a). However, stratiform rainfall also exhibits very different day-to-night rainfall variations. For example, daytime stratiform rainfall exceeds nighttime rainfall over most areas of the oceans, especially over the Pacific Ocean. Alternatively, stratiform rainfall over Africa and North America indicates generally lower contributions during daytime. The greater daytime stratiform contributions over the MSC regions, excepting North Africa, is also a salient feature. In addition, the seasonal variation of the spatial ratio patterns of daytime to nighttime stratiform rainfall denote that the mechanisms of this rainfall mode are more variable in time relative to their convective counterparts, depending on the precipitating system. In other words, convective rainfall does not exhibit as much seasonal dependence in its diurnal mechanisms. Notably, the day to night changes of stratiform rainfall can explain the total rainfall late evening secondary peak over continents and the afternoon secondary maximum over oceans, features originally discussed by Yang and Smith (2006) and Yang et al. (2006a) but only in terms of total rainfall.

The observed rainfall characteristics over the MSC areas are not in correspondence with a number of modeling studies. In fact, they are mostly contradictive from the modeling perspective in which a MSC drizzle minimum is supposed to occur during daytime along with a minimum in cloud cover (Turton and Nicholls 1987; Duynkerke 1989; Duynkerke and Hingnett 1993; Smith and Kao 1996; and Duynkerke and Teixeria 2001). This contradiction includes the case of

seasonal variability of MSC rainfall. Since precipitation over the major MSC domains is presumed to be mostly drizzle and warm rain, a spectral rainrate portion of which is not detectable by the TRMM PR (its inherent 17 dBZ sensitivity cuts off rainrates below the 0.25-0.3 m hr^{-1} threshold), the observed precipitation features discussed above over the MSC regions should be treated with some caution. In the meantime, we are currently analyzing a newer CloudSat 94 GHz Cloud Profiling Radar (CPR) dataset over the MCS regions, to confirm whether our TRMM results remain valid vis-à-vis total rainfall.

Figure 9 shows mean seasonal zonal profiles of convective and stratiform rainfall contributions during daytime and nighttime over ocean and continent for the 8-year 2a25 dataset (similar diagrams from the 2b31 algorithm are not shown). Over ocean (left-hand panels of Fig. 9), whereas there is considerable meridional variability in the relative daytime-nighttime contributions due to the two categories of rainfall, there is also considerable similarity in their respective zonal profiles from season-to-season, particularly in the high-amplitude rainfall zone. This indicates that the diurnally changing convective and stratiform rainfall mechanisms are consistently regulated, undergoing little modulation over time -- i.e., stationarity. However, the situation for the continental regime is quite different (right-hand panels of Fig. 9). The contribution by continental convective rainfall is much greater during daytime because the diurnal cycle of continental surface heating is so strong. In addition, the zonal profiles exhibit strong season-to-season variability -- even within the high-amplitude rainfall zone.

Tables 2a-b summarize the overall seasonal changes of oceanic and continental convective and stratiform rainfall contributions during daytime and nighttime based on the 8-year 2a25 and 2b31 datasets. The consistent agreement between algorithms 2a25 and 2b31 for both convective and stratiform categories are apparent. During daytime, the seasonal changes of convective and stratiform rainfall contributions are small over oceans, but clearly much greater over continents,

especially during the Autumn to Winter transition. Overall, convective and stratiform rainfall contributes some 41-44% and 56-59% over oceans, while about 54-55% and 45-46% over continents, respectively. During nighttime, the seasonal variations are small over oceans, but considerable over continents for both convective and stratiform rainfall. The nighttime convective and stratiform rainfall contributions are about 42-46% and 54-58% over ocean, while about 48-49% and 51-52% over land, respectively.

4.2 Diurnal Variations

Published studies on rainfall's diurnal cycle have almost exclusively focused on total rainfall. Studies of diurnal variability over the global tropics with categorized rainfall were effectively impossible prior to the TRMM era due to the lack of partitioned datasets. Yang and Smith (2006) and Yang et al. (2006a) analyzed the horizontal distributions and variations of precipitation's diurnal cycle at the global scale based on TRMM data, however, these studies did not consider convective and stratiform partitioning. Using eight years of partitioned TRMM data, helps shed light on various aspects of the root cause of diurnal variability of precipitation.

The diurnal variation of convective and stratiform rainfall from algorithm 2a25 is illustrated in Figure 10. Differences are prominent between the oceanic and continental rainfall regimes. Over oceans, convective rainfall exhibits the same diurnal cycle as total rainfall, while stratiform rainfall barely exhibits a secondary peak in the early afternoon, and only in Spring and Winter -- in addition to its primary morning maximum. The afternoon secondary peak of oceanic total rainfall is small in a globally-averaged framework. Over continents, the afternoon primary peak of convective rainfall mimics the diurnal behavior of total rainfall, while stratiform rainfall clearly exhibits a significant late evening maximum between 03-06 am Mean Solar Time (MST) along with the associated primary convective maximum between 15-18 pm MST.

Fig. 10 also shows the seasonal variations of the rainfall diurnal cycle, especially for oceanic precipitation. For example, the diurnal variation of total rainfall indicates a dominant peak during 03-06 am MST in Spring, and a broad late evening maximum in Summer, Autumn and Winter. Convective and stratiform rainfall indicate in-phase diurnal cycles in Spring, but not for the other seasons. Convective rainfall indicates a relatively stationary pattern of the diurnal cycle from season-to-season, whereas stratiform rainfall indicates strong seasonal variation. For continental rainfall, the seasonal variation in the diurnal cycle is more stationary for the primary afternoon peak, noting the late evening secondary peak appears stronger in Summer and Winter for both total rainfall and convective rainfall. This means there are changes from season-to-season in the overall continental diurnal cycle, but with peak amplitudes for the secondary mode remaining fairly stationary between 03-06 am MST for all seasons.

Comparisons of the overall seasonally diurnal variability for categorized rainfall over ocean and continent demonstrate that the dominant peak for total rainfall is mainly produced by the convective mode, especially for the continental case. Since the mid-to-late afternoon peak of continental convective rainfall is mostly forced by the diurnal cycle of solar radiation, the stationary afternoon primary peak of convective rainfall is understandable. However, the late evening secondary peak of continental rainfall is influenced by both convective and stratiform rainfall processes, especially the later. Moreover, over ocean, the dominant peak of rainfall's diurnal cycle is also mainly controlled by convective rainfall, but modulated by stratiform rainfall in a somewhat subtle fashion. These results suggest that the mechanisms behind rainfall's multi-mode diurnal cycle, at least in terms of the amplitudes and phases of the primary and secondary modes, are more complex over oceans than over continents. In any circumstance, the secondary maximum in rainfall's diurnal cycle at the global scale appears to be mostly impacted and modulated by stratiform rainfall.

Figure 11 presents mean seasonal relative contributions of convective and stratiform rainfall over the diurnal cycle from the 8-year 2a25 and 2b31 datasets. [The systematic agreements for convective and stratiform rainfall diurnal variations between the two algorithms are evident.] Overall, the consistency of greater stratiform oceanic rainfall is the prominent diurnal feature in this diagram. An afternoon peak in stratiform rainfall contribution and a late evening peak in convective rainfall contribution are apparent over oceans. Over continents, the prominent diurnal phenomena are an afternoon peak in convective rainfall contribution and a relatively greater late evening peak in stratiform rainfall contribution.

Figure 12 shows the relative contributions (as a percentage) of rainfall in each 3-hourly diurnal time interval with respect to total daily rainfall, for the 8-year 2a25 dataset, divided into mean seasonal total, convective, stratiform, and "other" rainfall categories. The relative changes of the percentages every 3 hours depict the diurnal loading of the categorized rainfall. The seasonal diurnal patterns are relatively stationary but with distinct characteristics associated with ocean and continent. Over oceans, the diurnal patterns are very similar for the different rain categories. This property is likely due to the fact that stratiform oceanic rainfall always accompanies convective rainfall. Thus all categories are nearly equally important from a loading perspective, but obviously not from a relative contribution perspective as the prior results testify. This type of diagram is just as effective as a rainrate diagram in emphasizing the modal maxima, which is why the primary oceanic mode is evident in both convective and stratiform categories (as well as in the "other" category), while only the stratiform loading exhibits the secondary mode. Over continents, there are exceedingly variable but stationary diurnal loading patterns for the four different rainfall categories. An afternoon primary peak and a late evening secondary peak of convective rainfall are stationary throughout the four seasons, as are these same peaks in total rainfall. By the same token, stratiform rainfall exhibits a late evening primary peak for all

seasons but only an afternoon secondary peak during Spring and Summer. It is worthwhile to point out that the "other" rainfall category exhibits a diurnal loading pattern similar to stratiform rainfall over oceans regardless that this category's rain amounts are very small, but with only one obvious delayed afternoon peak.

A synthesis of the diurnal behavior across the four rainfall categories indicates that the primary late evening peak of oceanic rainfall is due to organized convective systems, with stratiform rainfall inevitably associated with the convective component (as described by Houze 1997). In contrast, the afternoon primary peak of continental rainfall is mostly due to the convective mode alone. In addition, the stationary late evening secondary peak of stratiform rainfall over continents indicates that the diurnal cycle of total rainfall is strongly influenced and ultimately modulated by stratiform processes. In the case of oceans, the weak afternoon secondary peak is also due to modulation by diurnal stratiform processes, but not exclusive of accompanying convective processes. Thus, it would be more accurate to conclude that the dual mode behavior over oceans is a cooperative relationship between convective and stratiform processes, in which both modulate a primary mode with a nascent secondary mode -- but one which never achieves prominence at the global scale in a multi-year framework.

5.0 Regional and Interannual Variability

The results discussed previously point out that oceanic rainfall at the global scale in a multi-year framework exhibits an afternoon secondary peak, but one that is much weaker than its continental counterpart, and one that virtually disappears during the Autumn and Winter seasons. However, results from our previous study (Yang and Smith 2006) indicate that a well-defined secondary peak in oceanic total rainfall is apparent at the seasonal-regional scale for an individual year (1998). Thus, we analyze two 8-year TRMM datasets (i.e., from algorithms 2a25 and 2b31) at the regional scale followed by an analysis in an interannual framework, both

analyses designed to question if the secondary oceanic feature is consistently weak or is simply being smeared out by too much extended averaging.

To carry out the first analysis, six regional domains have been selected. Five of these are oceanic while one is continental. They are as follows: (1) West Pacific -- WP (5°S-5°N, 150-165°E); (2) East Pacific -- EP (10°N-20°N, 125°W-110°W); (3) Atlantic Ocean -- AO (Eq-10°N, 40°W-25°W); (4) Indian Ocean -- IO (5°S-5°N, 75°E-90°E); (5) South China Sea -- SCS (10°N-20°N, 110°E-120°E); and (6) Brazil Rain Forest -- BRF (15°S-Eq, 65°W-45°W). These domains are characterized by either climatological heavy rainfall or have been given special attention in recent field campaigns focused on major precipitation processes. For example, the West Pacific region is associated with the TRMM KWAJEX Experiment (Yuter *et al.* 2005); the South China Sea region is associated with the TRMM South China Sea Monsoon Experiment (Lau *et al.* 2000); and the Brazilian Rainforest region is associated with the TRMM Large Scale Biosphere-Atmosphere Experiment in the Amazon (LBA) (Halverson *et al.* 2002, Petersen *et al.* 2002).

Table 3 summarizes the mean contributions of seasonal convective and stratiform rainfall over these six regions from the two 8-year datasets. Both algorithms give rise to generally similar convective and stratiform rainfall contributions, with the most significant differences apparent over the Atlantic and Indian Ocean regions. These differences are linked to the different physical assumptions used in the two algorithms and the resultant regional biases that arise, see Berg et al. (2002) and Yang et al. (2006b) for discussions of possible causes of regional biases. Overall, there is more convective rainfall over the SCS and BRF domains, with more stratiform rainfall over the WP and EP domains. Seasonal variations of convective and stratiform rainfall are also evident, such as: (a) more stratiform rainfall in Spring, Summer and Winter over the WP domain; (b) more convective rainfall in Spring and Winter and more stratiform rainfall in Summer and Autumn over the EP domain; (c) more Summer stratiform rainfall and Winter convective rainfall

over the AO domain; (d) more convective rainfall in Spring and more stratiform rainfall in Autumn over the IO domain; (e) relatively more convective rainfall in all seasons over the SCS domain; and (f) much more convective rainfall (>60%) during the BRF dry season (Summer and Autumn). Among other things, these results demonstrate that stratiform rainfall is a very important component with respect to tropical precipitation generation.

Figure 13 shows the mean seasonal changes of the rainfall diurnal cycle over these six regions based on the 8-year 2b31 dataset. [The 2a25 dataset exhibits similar results.] The seasonal variations of rainfall amount are prominent because these regions are associated with movement of the ITCZ, activity in the Asian Monsoon, and variations in the wet-dry season cycle of the Brazilian Rainforest. The diurnal cycles of rainfall show dramatic seasonal variations in terms of the modal structure. The regional differences are also very obvious. Regardless of all the seasonal-regional variability, one salient feature is evident. There is consistency in the occurrence of the primary and secondary modes. The table 4 summarizes the presence or absence of the primary and secondary peaks in Fig 13, their relative amplitude given as one of three relative categories (strong, moderate, or weak), and whether a major delay in the timing (phase) of a given peak is evident. The contents of the table are easy to summarize. Of the 24 possible seasonal-regional cases, 23 indicate primary peaks with 9 of these exhibiting strong amplitudes and only 3 indicating weak amplitudes. For the secondary peaks, 19 are in evidence, with 3 strong and 6 weak. Of the 42 of 48 peaks in evidence, only 7 indicate significant phase delays from their notional positions.

The diurnal cycles of mean seasonal contributions for convective and stratiform rainfall from the 8-year 2b31 dataset are shown in Figure 14. This diagram is complex but helps reveal a few basic issues concerning regional variations. Two cases are examined in detail (the remainder are left for the reader). We first consider the continental BRF case, in which convective rainfall

indicates a stationary afternoon primary peak and weak secondary peaks in Spring and Winter, whereas stratiform rainfall indicates moderate to strong afternoon primary peaks and moderate late evening peaks. The convective component heavily dominates afternoon precipitation producing ~75% of the total during the dry season and ~60% during the wet season. Alternatively, stratiform rainfall contributes ~60% to the late evening total during the wet season and ~45% during the dry season. Seasonal changes in diurnal variability are consistent with the results from Machado et al. (2002, 2004) over the Amazônia rainforest domain based on LBA surface radar and satellite measurements.

An interesting maritime case is SCS. As shown in Table 4, rainfall in the SCS domain exhibits delayed primary and secondary peaks in Spring and Summer. Moreover, the delays are evident in both Spring and Summer for the primary convective mode (in which the secondary mode is not present), and in the primary stratiform mode (in which the secondary mode is present but weak). In contrast, the Autumn and Winter seasons exhibit strong and well phased primary and secondary peaks, emphasizing that the answer to the question at the beginning of the section is that the secondary oceanic mode can be very strong on a seasonal-regional basis.

Figure 15 presents the results from the interannual analysis to demonstrate that just as the secondary oceanic peak can be a major feature at regional scales, when the averaging is taken within an annual time frame even at the global scale, the oceanic secondary peak can be just as prominent. This is seen by noting that the abscissas of the two diagrams in Fig. 15 represent repeated diurnal cycles for the sequential annual intervals. Thus, for ocean there are very pronounced secondary peaks for the years 2002, 2003, and 2005, less pronounced secondary peaks for the years 1999 and 2000, and no secondary peaks for the years 1998, 2001, and 2004. It is also quite evident that whereas stratiform rainfall dominates the secondary peak structure, both convective and stratiform rainfall contribute to the primary mode. For continents, stratiform

rainfall modulates the behavior of the diurnal modes, especially the secondary late evening mode, while the primary diurnal peak is completely dominated by the convective component. As with oceanic rainfall, the secondary mode appears and disappears as a function of year when portrayed at the global scale.

6.0 Discussion and Conclusions

Eight years (1998-2005) of rainfall retrievals from three standard TRMM level 2 rainrate algorithms from TMI-only 2a12, PR-only 2a25, and combined PR-TMI 2b31 algorithms, have been used to analyze seasonal convective and stratiform rainfall variability at global and regional scales. The highly consistent behavior amongst these three algorithms, for mean horizontal rainfall distributions and for the underlying seasonal variations, confirms the intrinsic reliability of the TRMM rainfall products.

Seasonal rainfall variations correspond to well-known major climatic rainfall processes in the ITCZ, SPCZ, Asian Monsoon, tropical African/South American rainforests, subtropical maritime storm tracks, and subtropical South African / South American wet-dry regimes -- with accuracy and horizontal detail. As expected, the zonal mean rainfall patterns from 2a12, 2a25, and 2b31 exhibit small differences over both oceans and continents. The seasonal changes in zonal mean oceanic rainfall account for the seasonal movement of the ITCZ. The secondary peak in zonal mean rainfall during Winter is in response to SPCZ intensification, with the major peak corresponding to movement of the ITCZ into the SH. Seasonal changes in the zonal mean continental rainfall maxima are well correlated with Asian Monsoon activity and variations arising due to the wet-dry season cycles in South Africa and South America.

The overall contributions of oceanic convective and stratiform rainfall to total rainfall are ~42-55% and ~55-58%, respectively, while the contributions of continental convective and stratiform rainfall are ~52% and ~48%, respectively. The seasonal variations of oceanic

convective and stratiform rainfall contribution are small, ~2% for both, but up to ~11% for continents. Along with selected seasonal variations, there are significant variations in convective and stratiform rainfall contributions for both oceans and continents when the data are analyzed at the seasonal regional scale and the interannual global scale. In general, there is relatively more oceanic convective rainfall in areas of heavy rainfall and even over certain areas of weak rainfall, such as in the southeast Pacific Ocean, as well as over almost all tropical and subtropical continental areas. Conversely, stratiform rainfall is most dominant over subtropical ocean areas.

Seasonal rainfall exhibits significant diurnal variations in both the day-night framework and in the continuous diurnal cycle framework. Consistently greater daytime rainfall over continental and coastal areas and greater nighttime rainfall over open oceans are the principal features. Zonal distributions of daytime to nighttime rainfall ratio are stationary over the four seasons. In addition, daytime continental convective rainfall consistently exceeds nighttime rainfall over continents, whereas for oceans the reverse is true. On the other hand, seasonal stratiform rainfall exhibits a complex horizontal ratio distribution of daytime to nighttime rainfall. Also, there is no consistent behavior of the daytime to nighttime ratio for seasonal stratiform rainfall over either ocean or land. More daytime stratiform rainfall is found over some oceanic and continental regions, with the opposite true elsewhere, with seasonal changes apparent. These results suggest that the seasonal variation of stratiform rainfall is the important modulator of the afternoon secondary peak of oceanic rainfall and the late evening secondary peak of continental rainfall.

The generally greater daytime to nighttime rainfall over the MSC regions is in contradiction to many modeling results. It may seem odd that we find the apparent cause of the daytime MSC maximum to be due to stratiform rainfall when the pending controversy concerns a daytime convective overturning mode. This is simply due to the fact that the 2a23 convective-stratiform categorization algorithm cannot validly identify shallow warm rain as a convective process.

Instead, it is assigned to the stratiform category in keeping with the generally accepted definitions of the properties of stratiform rainfall. In any circumstance, these results indicate that modelers will have to pay greater attention to the mechanisms of both convective and stratiform precipitation within MSC environments.

Overall, seasonal oceanic rainfall exhibits a dominant late evening peak, while continental rainfall exhibits a dominant afternoon peak and a late evening secondary peak at the global scale in a multi-year framework. The in-phase relationship between the dominant convective rainfall peak and the dominant peak of total rainfall indicates that convective rainfall activities produce the overall primary diurnal mode of surface rainfall over both oceans and continents. Stratiform rainfall exhibits a small afternoon peak over oceans, and a clearly evident late evening peak over continents. Thus we conclude that stratiform rainfall is always modulating the rainfall diurnal cycle, in terms of the presence, amplitude, and phase of the secondary mode. Seasonal stationarity is a main feature of the primary peak of rainfall's diurnal cycle, but is not the case for the secondary peak, particularly in terms of the stratiform component. It is also noted that the small amounts of "other" oceanic rainfall exhibit a similar diurnal pattern to its stratiform counterpart, while its delayed afternoon peak over continents mimics the diurnal cycle of cloudiness over continents (Wylie and Woolf, 2002).

The diurnal cycles of rainfall over six selected regions exhibit distinct features as initially discussed in Yang and Smith (2006) and distinct seasonal variability. These results demonstrate that the seasonal-regional diurnal cycles of rainfall are strongly associated to the varying physics of precipitating cloud systems and storms, and to the atmospheric environments in which they develop. In fact, the relatively weak afternoon secondary peak of oceanic rainfall found at the global scale in the multi-year framework becomes very strong selectively at the seasonal-regional scale. Moreover, it is found that the amplitude of the secondary peak of oceanic rainfall

on a global scale varies between strong and weak (even non-existent) depending on the year, i.e., its interannually varying behavior -- all of which suggests that the secondary peak is an important property of global precipitation and one which global modelers need to address as modeling faces up to the task of replicating all but the simplest properties of global precipitation.

The underlying significance of the results is that they force a break with the past in the analysis of diurnal precipitation variability. Typically, and for over a century, studies of rainfall's diurnal variability have considered total rainfall almost exclusively. The appearance of secondary, tertiary, and even quaternary modes have never been explained theoretically (or even heuristically) with any consensus concerning cause [see Yang et al. 2007 (this issue) for detailed discussion on the secondary diurnal modes]. The results presented here demonstrate the importance of partitioning total rainfall into separate convective and stratiform components, and then recognizing that the behavior of separate diurnal modes largely arise from distinct diurnal stratiform variations modulating convective variations. This suggests, in essence, that stratiform variations are the underlying control on the amplitude and phase of the primary and secondary modes, and perhaps additional higher frequency modes. In our view, these properties of precipitation's diurnal variability will have to be considered in any future investigations concerning rainfall's diurnal cycle.

7.0 Acknowledgements

The authors wish to thank Dr. Erich Franz Stocker, Dr. John Kwiatkowski, Mr. John Stout, and additional members of the TRMM Science & Data Information System (TSDIS) staff for providing us the various TRMM rainfall products. This research has been supported by the NASA Precipitation Measurement Missions (PMM) Program under the management of Dr. Ramesh Kakar at NASA Headquarters.

8.0 References

Ackerman, S.A, and S.K. Cox, 1981: GATE phase III mean synoptic-scale radiative convergence profiles. *Mon. Wea. Rev.*, **109**, 371-383.

Awaka, J., T. Iguchi, H. Kumagai, and K. Okamoto, 1997: Rain type classification algorithm for TRMM Precipitation Radar. Proceedings of IGARSS'97, IEEE, Singapore, 1633-1635.

Awaka, J., T. Iguchi, and K. Okamoto, 2007: Rain type classification algorithm. *Measuring Precipitation from Space: EURAINSAT and the Future* (V. Levizzani, P. Bauer, and F.J. Turk, eds.), Springer, 213-224.

Berg, W., C. Kummerow, and C. Morales, 2002: Differences between East and West Pacific rainfall systems. *J. Clim*, **15**, 3659-3672.

Betts, A.K., 1982: Saturation point analysis of moist convective overturning. *J. Atmos. Sci.*, **39**, 1484-1505.

Dai, A., 2001: Global precipitation and thunderstorm frequencies. Part II: Diurnal variations. *J. Clim.*, **14**, 1112-1128.

Duynkerke, P.G., 1989: The diurnal variation of a marine stratrocumulus layer: A model sensitivity study. *Mon. Wea. Rev.*, **117**, 1710-1725.

Duynkerke, P.G., and P. Hignett, 1993: Simulation of diurnal variation in a stratocumulus-capped marine boundary layer during FIRE. *Mon. Wea. Rev.*, **121**, 3291-3300.

Duynkerke, P.G., and J. Teixeira, 2001: Comparison of the ECMWF reanalysis with FIRE I observations: Diurnal variation of marine stratocumulus. *J. Clim.*, **14**, 1466-1478.

Ebert, E.E., and M.J. Manton, 1998: Performance of satellite rainfall estimation algorithms during TOGA COARE. *J. Atmos. Sci.*, **55**,1537-1557.

Emanuel, K., 1986: An air-sea interaction theory of tropical cyclones. Part I: Steady state maintenance. *J. Atmos. Sci.*, **43**, 584-604.

Emanuel, K., 1994: *Atmospheric Convection*. Oxford University Press, New York, 580 pp

Foltz, G.S., and W.M. Gray, 1979: Diurnal variations in the troposphere's energy balance. *J. Atmos. Sci.*, **36**, 1450-1466.

Geerts, B., and Y. Dawei, 2004: Classification and characterization of tropical precipitation based on high-resolution airborne vertical incidence radar. Part I: Classification. *J. Appl. Meteor.*, **43**, 1554-1566.

Gray, W.M., and R.W. Jacobson, Jr., 1977: Diurnal variation of deep cumulus convection. *Mon. Wea. Rev.*, **105**, 1171-1188.

Haddad, Z.S., E.A. Smith, C.D. Kummerow, T. Iguchi, M.R. Farrar, S.L. Durden, M. Alves, and W.S. Olson, 1997: The TRMM 'Day-1' radar/radiometer combined rain-profile algorithm. *J. Meteor. Soc. Japan*, **75**, 799-809.

Haddad, Z.S., J.P. Meagher, R.F.Adler, E.A. Smith, E. Im, and S.L. Durden, 2004: El Niño and the variability of global precipitation. *J. Geophys. Res.*, **109**, D17103, 7 pp.

Halverson, J.B., T. Rickenbach, B. Roy, H. Pierce, and E. Williams, 2002: Environmental characteristics of convective systems during TRMM-LBA. *Mon. Wea. Rev.*, **130**, 1493–1509.

Hann, J., 1901: *Lehrbuch der Meteorologie* (1st ed). Chr. Herm Tachnitz, Leipzig, 338-346.

Hirose, M., and K. Nakamura, 2005: Spatial and diurnal variation of precipitation systems over Asia observed by the TRMM Precipitation Radar. *J. Geophys. Res.*, **110**, Do5106, doi:10.1029/2004JD004815.

Hou, A.Y., S.Q. Zhang, and O. Reale, 2004: Variational continuous assimilation of TMI and SSM/I rain rates: Impact on GEOS-3 hurricane analyses and forecasts. *Mon. Wea. Rev.*, **132**, 2094-2109.

Houze, R.A., Jr., 1989: Observed structure of mesoscale convective systems and implications for large-scale heating. *Quart. J. Roy. Meteor. Soc.*, **115**, 427-461.

Houze, R.A., Jr., 1997: Stratiform precipitation in regions of convection: A meteorological paradox. *Bull. Amer. Meteor. Soc.*, **78**, 2179-2196.

Huffman, G.J., R.F. Adler, P. Arkin, A. Chang, R. Ferraro, A. Gruber, J. Janowiak, A. McNab, B. Rudolf, and U. Schneider, 1997: The Global Precipitation Climatology Project (GPCP) combined precipitation data set. *Bull. Amer. Meteor. Soc.*, **78**, 5-20.

Iguchi, T., and R. Meneghini, 1994: Intercomparison of single-frequency methods for retrieving a vertical rain profile from airborne or spaceborne radar data. *J. Atmos. Oceanic Tech.*, **11**, 1507-1511.

Iguchi, T., T. Kozu, R. Meneghini, J. Awaka, and K. Okamoto, 2000: Rain-profiling algorithm for the TRMM precipitation radar. *J. Appl. Meteor.*, **39**, 2038-2052.

Janowiak, J.E., 1992: Tropical rainfall: A comparison of satellite-derived rainfall estimates with model precipitation forecasts, climatologies, and observations. *Mon. Wea. Rev.*, **120**, 448-462.

Johnson, R.H., and P.J. Hamilton, 1988: The relationship of surface pressure features to the precipitation and airflow structure of an intense midlatitude squall line. *Mon. Wea. Rev.*, **116**, 1444-1472.

Kraus, E.B., 1963: The diurnal precipitation change over the sea. *J. Atmos. Sci.*, **20**, 546-551.

Krishnamurti, T.N., S. Surendran, D.W. Shin, R.J. Correa-Torres, T.S.V.V. Kumar, E. Williford, C. Kummerow, R.F. Adler, J. Simpson, R. Kakar, W.S. Olson, and F.J. Turk, 2001: Real-time multianalysis-multimodel superensemble forecasts of precipitation using TRMM and SSM/I products. *Mon. Wea. Rev.*, **129**, 2861-2883.

Kummerow, C., W. Barnes, T. Kozu, J. Shiue, and J. Simpson, 1998: The Tropical Rainfall Measuring Mission (TRMM) sensor package. *J. Atmos. Oceanic Tech.*, **15**, 809-817.

Kummerow, C., J. Simpson, O. Thiele, W. Barnes, A.T.C. Chang, E. Stocker, R.F. Adler, A. Hou, R. Kakar, F. Wentz, P. Ashcroft, T. Kozu, Y. Hong, K. Okamoto, T. Iguchi, H. Kuroiwa, E. Im, Z. Haddad, G. Huffman, B. Ferrier, W.S. Olson, E. Zipser, E.A. Smith, T.T. Wilheit, G. North, T. Krishnamurti, and K. Nakamura, 2000: The status of the Tropical Rainfall Measuring Mission (TRMM) after two years in orbit. *J. Appl. Meteor.*, **39**, 1965-1982.

Kummerow, C., Y. Hong, W.S. Olson, S. Yang, R.F. Adler, J. Mccollum, R. Ferraro, G. Petty, and T.T. Wilheit, 2001: The evolution of the Goddard Profiling Algorithm (GPROF) for rainfall estimation from passive microwave sensors. *J. Appl. Meteor.*, **40**, 1801-1820.

Lau, K.M., Y. Ding, J.-T. Wang, R. Johnson, T. Keenan, R. Cifelli, J. Gerlach, O. Thiele, T. Rickenbach, S.-C. Tsay, and P.-H. Lin, 2000: A report of the field operations and early results of the South China Sea Monsoon Experiment (SCSMEX). *Bull. Amer. Meteor. Soc.*, **81**, 1261-1270.

Lavoie, R.L., 1963: *Some Aspects of Meteorology of the Tropical Pacific Viewed from an Atoll.* Rep. No. 27, Institute of Geophysics, Univ. of Hawaii, 76 pp.

L'Ecuyer, T.S., and G.L. Stephens, 2002: An estimation-based precipitation retrieval algorithm for attenuating radars. *J. Appl. Meteor.*, **41**, 272-285.

Lin, X., D.A. Randall, and L.D. Fowler, 2000: Diurnal variability of the hydrologic cycle and radiative fluxes: Comparisons between observations and a GCM. *J Clim.*, **13**, 4159-4179.

Machado, L.A.T., H. Laurent, and A. Lima, 2002: Diurnal march of the convection observed during TRMM-WETAMC/LBA. *J. Geophy. Res.*, **107(D20)**, 8064, doi: 10.1029/2001JD000338.

Machado, L.A.T., H. Laurent, N. Dessay, and I. Miranda, 2004: Seasonal and diurnal variability of convection over the Amazonia: A comparison of different vegetation types and large scale forcing. *Theor. Appl. Climatol.*, **78**, 61-77.

McBride, J.L., and W.M. Gray, 1980: Mass divergence in tropical weather systems. Part I: Diurnal variation. *Quart. J. Roy. Meteor. Soc.*, **106**, 501-516.

Meneghini, R., and T. Kozu, 1990: *Spaceborne Weather Radar.* Artech House, 199 pp.

Meneghini, R., T. Iguchi, T. Kozu, L. Liao, K. Okamoto, J. Jones, and J. Kwiatkowski, 2000: Use of the surface reference technique for path attenuation estimates from the TRMM Precipitation Radar. *J. Appl. Meteor.*, **39**, 2053-2070.

Negri, A.J., T.L. Bell, and L. Xu, 2002: Sampling of the diurnal cycle of precipitation using TRMM. *J. Atmos. Oceanic Technol.*, **19**, 1333-1344.

Olson, W.S., C.D. Kummerow, S. Yang, G.W. Petty, W.-K. Tao, T.L. Bell, S.A. Braun, Y. Wang, S.E. Lang, D.E. Johnson, and C. Chiu, 2006: Precipitation and latent heating distributions from satellite passive microwave radiometry. Part I: Improved method and uncertainty estimates. *J. Appl. Meteor.*, **45**, 702-720.

Petersen, W.A., S.W. Nesbitt, R.J. Blakeslee, R. Cifelli, P. Hein, and S.A. Rutledge, 2002: TRMM observations of intraseasonal variability in convective regimes over the Amazon. *J. Clim.*, **15**, 1278–1294.

Ramage, C.S., 1971: *Monsoon Meteorology.* Academic Press, New York, 295 pp.

Randall, D.A., Harshvardhan, and D.A. Dazlich, 1991: Diurnal variability of the hydrologic cycle in a general circulation model. *J. Atmos. Sci.*, **48**, 40-62.

Rasmusson, E.M., and P.A. Arkin, 1993: A global view of large-scale precipitation variability. *J. Clim.*, **6**, 1495-1522.

Ruprecht, E., and W.M. Gray, 1976: Analysis of satellite-observed cloud clusters: Papers I and II. *Tellus*, **28**, 391-425.

Rutledge, S.A., and R.A. Houze, Jr., 1987: A Diagnostic Modelling Study of the Trailing Stratiform Region of a Midlatitude Squall Line. *J. Atmos. Sci.*, **44**, 2640-2656.

Schumacher, C., and R.A. Houze, Jr., 2003: Stratiform rain in the tropics as seen by the TRMM Precipitation Radar. *J. Clim.*, **16**, 1739-1756.

Schumacher, C., R.A. Houze, Jr., and I. Kraucunas, 2004: The tropical dynamical response to latent heating estimates derived from the TRMM precipitation radar. *J. Atmos. Sci.*, **61**, 1341-1358.

Shinoda, T., and R. Lukas, 1995: Lagrangian mixed layer modeling of the western equatorial Pacific. *J. Geophys. Res.*, **100**, 2523-2541.

Short, D.A., P.A. Kucera, B.S. Ferrier, J.C. Gerlach, S.A. Rutledge, and O.W. Thiele, 1997: Shipboard radar rainfall patterns within the TOGA/COARE IFA. *Bull. Amer. Meteor. Soc.*, **78**, 2817-2836.

Short, D.A. and K Nakamura, 2000: TRMM radar observations of shallow precipitation over the tropical oceans. *J. Clim.*, **13**, 4107- 4124.

Simpson, J., C. Kummerow, W.-K. Tao, and R. Adler, 1996: On the Tropical Rainfall Measuring Mission (TRMM). *Meteorol. Atmos. Phys.*, **60**, 19-36.

Simpson, J., R.F. Adler, and G. North, 1988: A proposed Tropical Rainfall Measuring Mission (TRMM) satellite. *Bull. Amer. Meteor. Soc.*, **69**, 278-295.

Smith, W.S., and C.-Y.J. Kao, 1996: Numerical simulations of the marine stratocumulus-capped boundary layer and its diurnal variation. *Mon. Wea. Rev.*, **124**, 1803-1816.

Smith, E.A., J. Turk, M. Farrar, A. Mugnai, and X. Xiang, 1997: Estimating 13.8 GHz path integrated attenuation from 10.7 GHz brightness temperatures for TRMM combined PR-TMI precipitation algorithm. *J. Appl. Meteor.*, **36**, 365-388.

Smith, E.A., J. Lamm, R. Adler, J. Alishouse, K. Aonashi, E. Barrett, P. Bauer, W. Berg, A. Chang, R. Ferraro, J. Ferriday, S. Goodman, N. Grody, C. Kidd, D. Kniveton, C. Kummerow, G. Liu, F. Marzano, A. Mugnai, W. Olson, G. Petty, A. Shibata, R. Spencer, F. Wentz, T. Wilheit, and E. Zipser, 1998: Results of WetNet PIP-2 project. *J. Atmos. Sci.*, **55**, 1483-1536.

Smith, E.A., G. Asrar, Y. Furuhama, A. Ginati, A. Mugnai, K. Nakamura, R. Adler, M.-D. Chou, M. Desbois, J. Durning, F. Einaudi, J. Entin, R. Ferraro, R. Guzzi, P. Houser, P. Hwang, T Iguchi, P. Joe, R. Kakar, J. Kaye, M. Kojima, C. Kummerow, K.-S. Kuo, D. Lettenmaier, V. Levizzani, N. Lu, A. Mehta, C. Morales, P. Morel, T. Nakazawa, S. Neeck, K. Okamoto, R. Oki, G. Raju, J.M. Shepherd, J. Simpson, B.-J. Sohn, E.F. Stocker, W.-K. Tao, J. Testud, G. Tripoli, E. Wood, S. Yang, and W. Zhang, 2007: International Global Precipitation Measurement (GPM) Program and Mission: An overview. *Measuring Precipitation from Space: EURAINSAT and the Future* (V. Levizzani, P. Bauer, and F.J. Turk, eds.), Springer 611-654.

Smith, E.A., A. Mehta, S. Yang, A. Mugnai, and G.J. Tripoli, 2007: Sequential diurnal - quasigeostrophic propagation of warm season precipitation due to formation of mountain slope flows and front plains MCSs. *J. Clim.*, this issue.

Steiner, M., R.A. Houze, Jr., and S.E. Yuter, 1995: Climatological characterization of three-dimensional storm structure from operational radar and rain gauge data. *J. Appl. Meteor.*, 34, 1978-2007.

Stephens, G.L., D.G. Vane, R.J. Boain, G.G. Mace, K. Sassen, Z. Wang, A.J. Illingworth, E.J. O'Connor, W.B. Rossow, S.L. Durden, S.D. Miller, R.T. Austin, A. Benedetti, C. Mitrescu, and CloudSat Science Team, 2002: The CloudSat mission and the A-Train: A new dimension of space-based observations of clouds and precipitation. *Bull. Amer. Meteor. Soc.*, **83**, 1771-1790.

Sui, C.-H., K.-M. Lau, Y.N. Takayabu, and D.A. Short, 1997: Diurnal variations in tropical oceanic cumulus convection during TOGA COARE. *J. Atmos. Sci.*, **54**, 639-655.

Sui, C.-H., K.-M. Lau, and X. Li, 1998: Convective-radiative interaction in simulated diurnal variations of tropical cumulus ensemble. *J. Atmos. Sci.*, **55**, 2345-2357.

Tao, W.-K., C.-H. Sui, B. Ferrier, S. Lang, J. Scala, M.-D. Chou, and K. Pickering, 1993: Heating, moisture, and water budgets of tropical and midlatitude squall lines: Comparisons and sensitivity to longwave radiation. *J. Atmos. Sci.*, **50**, 673-690.

Tao, W.-K., S. Lang, J. Simpson, C.-H. Sui, B. Ferrier, and M.-D. Chou, 1996: Mechanisms of cloud-radiation interaction in the tropics and midlatitudes. *J. Atmos. Sci.*, **53**, 2624-2651.

Tao, W.-K., S. Lang, J. Simpson, W.S. Olson, D. Johnson, B. Ferrier, C. Kummerow, and R. Adler, 2000: Retrieving vertical profiles of latent heat release in TOGA COARE convective systems using a cloud resolving model, SSM/I and radar data. *J. Meteor. Soc. Japan*, **78**, 333-355.

Tao, W.-K., E.A. Smith, R.F. Adler, Z.S. Haddad, A.Y. Hou, T. Iguchi, R. Kakar, T.N. Krishnamurti, C.D. Kummerow, S. Lang, R. Meneghini, K. Nakamura, T. Nakazawa, K. Okamoto, W.S. Olson, S. Satoh, S. Shige, J. Simpson, Y. Takayabu, G.J. Tripoli, and S. Yang, 2006: Retrieval of latent heating from TRMM satellite measurements. *Bull. Amer. Meteor. Soc.*, **87**, 1555-1572.

Tremblay, A., 2005: The stratiform and convective components of surface precipitation. *J. Atmos. Sci.*, **62**, 1513-1528.

TSDIS, 2006: Tropical Rainfall Measuring Mission (TRMM) Science Data and Information System (TSDIS). Volume 4: File Specifications for TRMM products level 2 and level 3 (release 6.07). NASA/Goddard Space Flight Center TSDIS documents. [http:// tsdis.gsfc.nasa.gov/tsdis/tsdis_redesign/SelectedDocs.html]

Turton, J.D., and S. Nicholls, 1987: A study of the diurnal variations of stratocumulus using a multiple mixed layer model. *Quart. J. Roy. Meteor. Soc.*, **113**, 969-1009.

Wilheit, T., R. Adler, S. Avery, E. Barrett, P. Bauer, W. Berg, A. Chang, J. Ferriday, N. Grody, S. Goodman, C. Kidd, D. Kniveton, C. Kummerow, A. Mugnai, W. Olson, G. Petty, A. Shibata, E. Smith, and R. Spencer, 1994: Algorithms for the retrieval of rainfall from passive microwave measurements. *Remote Sensing Rev.*, **11**, 163-194.

Wolff, D.B., D.A. Marks, E. Amitai, D.S. Silberstein, B.L. Fisher, A. Tokay, J. Wang, and J.I. Pippitt , 2005: Ground validation for the tropical rainfall measuring mission (TRMM). *J. Atmos. Oceanic Tech.*, **22**, 365-380.

Wylie, D.P., and H.M. Woolf, 2002: The diurnal cycle of upper-tropospheric clouds measured by GOES-VAS and the ISCCP. *Mon. Wea. Rev.*, **130**, 171–179.

Xu, K., and K.A. Emanuel, 1989: Is the tropical atmosphere conditionally unstable? *Mon. Wea. Rev.*, **117**, 1471-1479.

Yang, S., and E. A. Smith, 1999a: Moisture budget analysis of TOGA-COARE area using SSM/I retrieved latent heating and large scale Q_2 estimates. *J. Atmospheric and Oceanic Technology*, **16**, 633-655.

Yang, S., and E.A. Smith, 1999b: Four dimensional structure of monthly latent heating derived from SSM/I satellite measurements. *J. Clim.*, **12**, 1016-1037.

Yang, S., and E.A. Smith, 2000: Vertical structure and transient behavior of convective-stratiform heating in TOGA-COARE from combined satellite-sounding analysis. *J. Appl. Meteor.*, **39**, 1491-1513.

Yang, S., and E.A. Smith, 2006: Mechanisms for diurnal variability of global tropical rainfall observed from TRMM. *J. Clim*, **19**, 5190-5226.

Yang, S., E.A. Smith, and K.-S. Kuo, 2006a: Diurnal variability of precipitation from TRMM measurements. *Remote Sensing and Modeling of the Atmosphere, Oceans, and Interactions* [T.N. Krishnamurti, B.N. Goswami, and T. Iwasaki, eds.], *Proc. SPIE*, **6404**, 64040I1-6.

Yang, S., W. Olson, J.J. Wang, T.L. Bell, E.A. Smith, and C.D. Kummerow, 2006b: Precipitation and latent heating distributions from satellite passive microwave radiometry. Part II: Evaluation of estimates using independent data. *J. Appl. Meteor.*, **45**, 721-739.

Yang S., E.A. Smith, and K.-S. Kuo, 2007: Persistent nature of secondary diurnal modes in both land and ocean precipitation. *J. Clim.*, this issue.

Yuter, S.E., R.A. Houze, Jr., E.A. Smith, T.T. Wilheit, and E. Zipser, 2005: Physical characterization of tropical oceanic convection observed in KWAJEX. *J. Appl. Meteorl.*, **44**, 385-415.

List of Tables

Table 1: Mean contributions (%) of seasonal/annual rainfall from eight years (1998-2005) of TRMM 2a25 and 2b31 algorithm retrievals over ocean and continent. [Convective, stratiform and "other" rainfall types are denoted by C, S, and O, respectively.]

Table 2a: Mean contributions (%) of seasonal/annual daytime rainfall from eight years of 2a25 and 2b31 algorithm retrievals over ocean and continent -- with daytime covering period from 06 am to 06 pm MST. [C, S, and O are defined in Table 1 legend.]

Table 2b: Same as in Table 2a except for nighttime rainfall, with nighttime covering period from 06 pm to 06 am MST.

Table 3: Mean contributions (%) of seasonal/annual rainfall from eight years of 2a25 and 2b31 algorithm retrievals over six selected regions: WP -- West Pacific (5°S-5°N ; 150°-165°E); EP -- East Pacific (10°N-20°N ; 125°-110°W); AO -- Atlantic Ocean (Eq-10°N ; 40°-25°W); IO -- Indian Ocean (5°S-5°N ; 75°-90°E); SCS -- South China Sea (10°-20°N ; 110°-120°E); BRF -- Brazil Rainforest (15°S-Eq ; 65°-45°W). [C, S, and O are defined in Table 1 legend.]

Table 4: Summary of presence (yes - Y ; no - N) and relative amplitude (strong - S ; moderate - M ; weak - W) of primary and secondary peaks in six regional domains (WP, EP, AO, IO, SCS, BRF) for four cardinal seasons. If (d) is indicated in either "Presence" column, this denotes major delay in onset of maximum relative to typical phase times for either primary or secondary modes.

Table 1: Mean contributions (%) of seasonal/annual rainfall from eight years (1998-2005) of TRMM 2a25 and 2b31 algorithm retrievals over ocean and continent. [Convective, stratiform and "other" rainfall types are denoted by C, S, and O, respectively.]

Rain Alg	Rain Type	Ocean					Continent				
		Spring	Summer	Autumn	Winter	Annual	Spring	Summer	Autumn	Winter	Annual
2a25	C	45.0	44.8	45.2	44.1	44.8	51.8	51.8	53.2	49.3	51.5
	S	54.9	55.1	54.7	55.8	55.1	48.0	48.0	46.7	50.6	48.3
	O	0.1	0.1	0.1	0.1	0.1	0.2	0.2	0.1	0.1	0.2
2b31	C	41.8	41.8	42.0	40.7	41.5	51.4	51.7	54.0	49.0	51.6
	S	58.1	58.1	57.9	59.2	58.4	48.5	48.2	45.9	50.9	48.3
	O	0.1	0.1	0.1	0.1	0.1	0.1	0.1	0.1	0.1	0.1

Table 2a: Mean contributions (%) of seasonal/annual daytime rainfall from eight years of 2a25 and 2b31 algorithm retrievals over ocean and continent -- with daytime covering period from 06 am to 06 pm MST. [C, S, and O are defined in Table 1 legend.]

Rain Alg	Rain Type	Ocean					Continent				
		Spring	Summer	Autumn	Winter	Annual	Spring	Summer	Autumn	Winter	Annual
2a25	C	44.1	43.9	44.2	42.8	43.7	54.9	54.4	57.3	53.7	55.1
	S	55.8	56.0	55.7	57.1	56.2	44.9	45.5	42.5	46.2	44.8
	O	0.1	0.1	0.1	0.1	0.1	0.2	0.1	0.2	0.1	0.1
2b31	C	41.0	40.9	41.0	39.6	40.6	53.6	53.5	57.6	52.8	54.4
	S	58.9	59.0	58.9	60.3	59.3	46.3	46.4	42.3	47.1	45.5
	O	0.1	0.1	0.1	0.1	0.1	0.1	0.1	0.1	0.1	0.1

Table 2b: Same as in Table 2a except for nighttime rainfall, with nighttime covering period from 06 pm to 06 am MST.

Rain Alg	Rain Type	Ocean					Continent				
		Spring	Summer	Autumn	Winter	Annual	Spring	Summer	Autumn	Winter	Annual
2a25	C	45.8	45.7	46.3	45.4	45.8	48.7	49.4	49.2	44.8	48.1
	S	54.1	54.2	53.6	54.5	54.1	51.1	50.5	50.6	55.0	51.8
	O	0.1	0.1	0.1	0.1	0.1	0.2	0.1	0.2	0.2	0.1
2b31	C	42.5	42.6	42.9	41.7	42.4	49.1	49.9	50.6	45.0	48.7
	S	57.4	57.3	57.0	58.2	57.5	50.8	50.0	49.3	54.9	51.2
	O	0.1	0.1	0.1	0.1	0.1	0.1	0.1	0.1	0.1	0.1

Table 3: Mean contributions (%) of seasonal/annual rainfall from eight years of 2a25 and 2b31 algorithm retrievals over six selected regions: WP -- West Pacific (5°S-5°N ; 150°-165°E); EP -- East Pacific (10°N-20°N ; 125°-110°W); AO -- Atlantic Ocean (Eq-10°N ; 40°-25°W); IO -- Indian Ocean (5°S-5°N ; 75°-90°E); SCS -- South China Sea (10°-20°N ; 110°-120°E); BRF -- Brazil Rainforest (15°S-Eq ; 65°-45°W). [C, S, and O are defined in Table 1 legend.]

		WP		EP		AO		IO		SCS		BRF	
		2a25	2b31	2a25	2b31	2a25	2b31	2a25	2b31	2a25	2b31	2a25	2b31
Spring	C	44.8	42.0	54.2	51.3	50.2	46.3	54.6	51.5	58.9	57.9	50.8	49.5
	S	55.2	58.0	45.6	48.6	49.7	53.6	45.3	48.4	41.0	42.0	49.1	50.5
	O	0	0	0.2	0.1	0.1	0.1	0.1	0.1	0.1	0.1	0.1	0
Summer	C	49.7	46.5	43.6	41.4	47.1	43.7	51.1	47.4	53.4	53.3	68.8	67.6
	S	50.2	53.4	56.3	58.5	52.8	56.3	48.8	52.6	46.5	46.7	31.0	32.4
	O	0.1	0.1	0.1	0.1	0.1	0	0.1	0	0.1	0.0	0.2	0
Autumn	C	52.4	48.9	43.8	40.5	50.8	47.4	46.8	43.1	54.0	53.8	62.7	65.1
	S	47.5	51.0	56.1	59.4	49.2	52.6	53.2	56.9	45.9	46.1	37.1	34.8
	O	0.1	0.1	0.1	0.1	0	0	0	0	0.1	0.1	0.2	0.1
Winter	C	47.5	44.8	52.8	50.3	53.7	50.2	51.7	49.0	55.2	53.2	49.0	49.1
	S	52.4	55.1	47.1	49.6	46.3	49.7	48.2	51.0	44.7	46.7	50.9	50.9
	O	0.1	0.1	0.1	0.1	0	0.1	0.1	0	0.1	0.1	0.1	0
Annual	C	48.3	45.3	46.0	43.3	50.3	46.8	50.7	47.4	54.6	54.1	54.2	54.6
	S	51.6	54.6	53.9	56.6	49.7	53.2	49.2	52.5	45.3	45.8	45.7	45.4
	O	0.1	0.1	0.1	0.1	0	0	0.1	0.1	0.1	0.1	0.1	0

Table 4: Summary of presence (yes - Y ; no - N) and relative amplitude (strong - S ; moderate - M ; weak - W) of primary and secondary peaks in six regional domains (WP, EP, AO, IO, SCS, BRF) for four cardinal seasons. If (d) is indicated in either "Presence" column, this denotes major delay in onset of maximum relative to typical phase times for either primary or secondary modes.

		Primary Peak		Secondary Peak	
Season	**Region**	**Presence**	**Relative Amplitude**	**Presence**	**Relative Amplitude**
Spring	**WP**	Y	S	Y	M
	EP	N	--	Y	W
	AO	Y	W	N	--
	IO	Y	M	Y	M
	SCS	Y(d)	M	N	--
	BRF	Y	S	Y	W
Summer	**WP**	Y	S	Y	M
	EP	Y (d)	M	Y (d)	M
	AO	Y	M	N	--
	IO	Y	W	Y	W
	SCS	Y (d)	S	Y (d)	W
	BRF	Y	S	N	--
Autumn	**WP**	Y	M	Y (d)	M
	EP	Y	M	Y	M
	AO	Y	M	Y	W
	IO	Y	M	Y	S
	SCS	Y	S	Y	S
	BRF	Y	S	N	--
Winter	**WP**	Y	M	Y	M
	EP	Y	W	Y	W
	AO	Y	M	Y	M
	IO	Y	M	Y (d)	M
	SCS	Y	S	Y	S
	BRF	Y	S	Y	M

List of Figures

Fig 9: Zonal mean seasonal convective and stratiform rainfall contributions (%) during daytime (D) and nighttime (N) over (a) ocean and (b) continent for 8-years of rainrate measurements from algorithm 2a25.

Fig 10: Diurnal cycle of mean seasonal rainfall (mm day^{-1}) partitioned into total (T), convective (C), and stratiform (S) categories over ocean (left panel) and continent (right panel) for 8-years of rainrate measurements from algorithm 2a25.

Fig 11: Diurnal cycle of mean seasonal convective and stratiform rainfall contributions at each 3-hourly diurnal time interval (%) over ocean (left panels) and continent (right panels) for 8-years of rainrate measurements from algorithms 2a25 and 2b31.

Fig 12: Diurnal cycle of relative contributions of rainfall in each 3-hourly diurnal time interval to total daily rainfall (%) for mean seasonal total (T), convective (C), stratiform (S), and "other" (O) rainfall over ocean (left panels) and continent (right panels) for 8-years of rainrate measurements from algorithm 2a25.

Fig 13: Diurnal variations of mean seasonal surface rainfall (mm day^{-1}) for 8-years of rainrate measurements from algorithm 2b31 over six regional domains: West Pacific (WP), East Pacific (EP), Atlantic Ocean (AO), Indian Ocean (IO), South China Sea (SCS), and Brazilian Rain Forest (BRF).

Fig 14: Diurnal variations of mean seasonal contributions (%) for convective (left panels) and stratiform (right panels) rainfall for 8-years of rainrate measurements from algorithm 2b31 over six regional domains identified in Fig. 13.

Fig 15: Interannual variability of mean oceanic and continental diurnal rainfall variability for total, convective, and stratiform rainfall categories for eight year TRMM 2b31. Each yearly segment on abscissa denotes 24-hour diurnal cycle from 00 to 24 MST. Left-hand (right) ordinates are assigned to convective and stratiform rainfall (total) variables (Unit: mm day^{-1}).

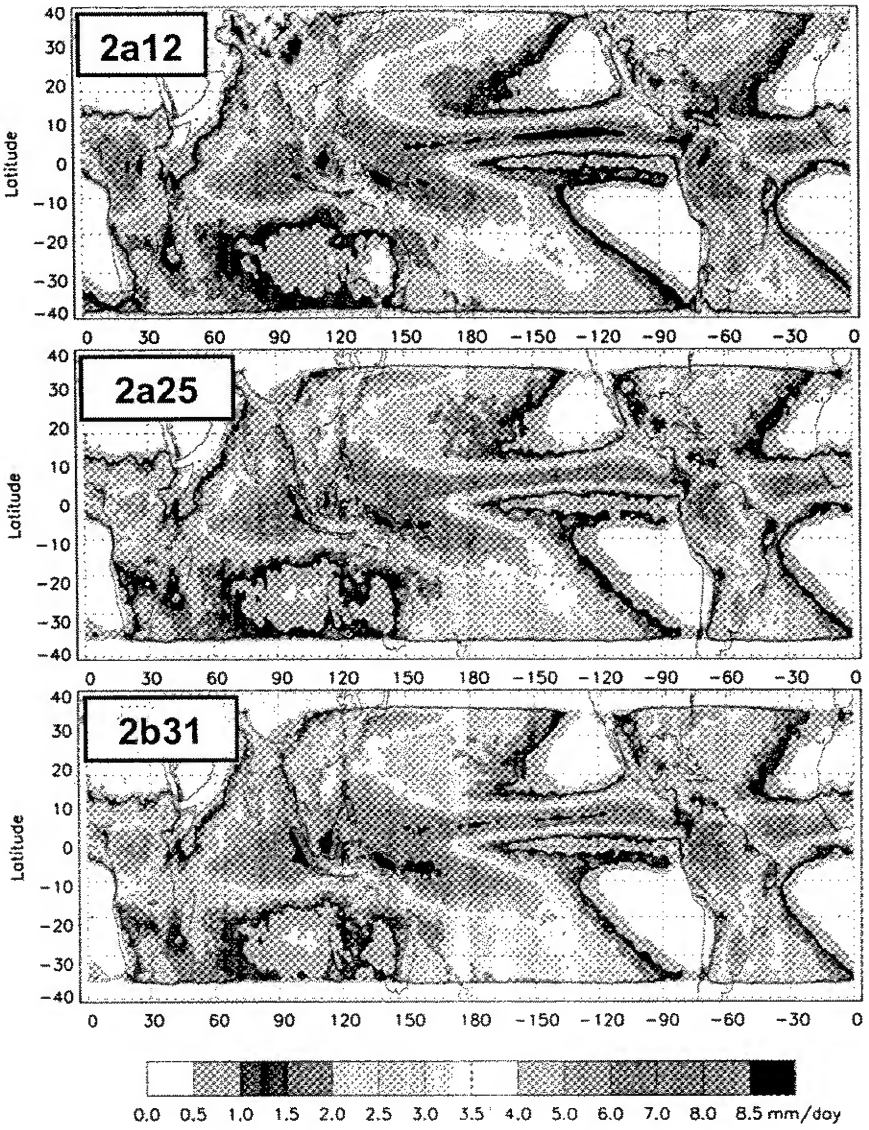

Figure 1: Horizontal distributions of 8-year (1998-2005) mean rainrate (mm day^{-1}) from TMI, PR, and combined PR-TMI algorithms 2a12 (upper panel), 2a25 (middle panel), and 2b31 (lower panel).

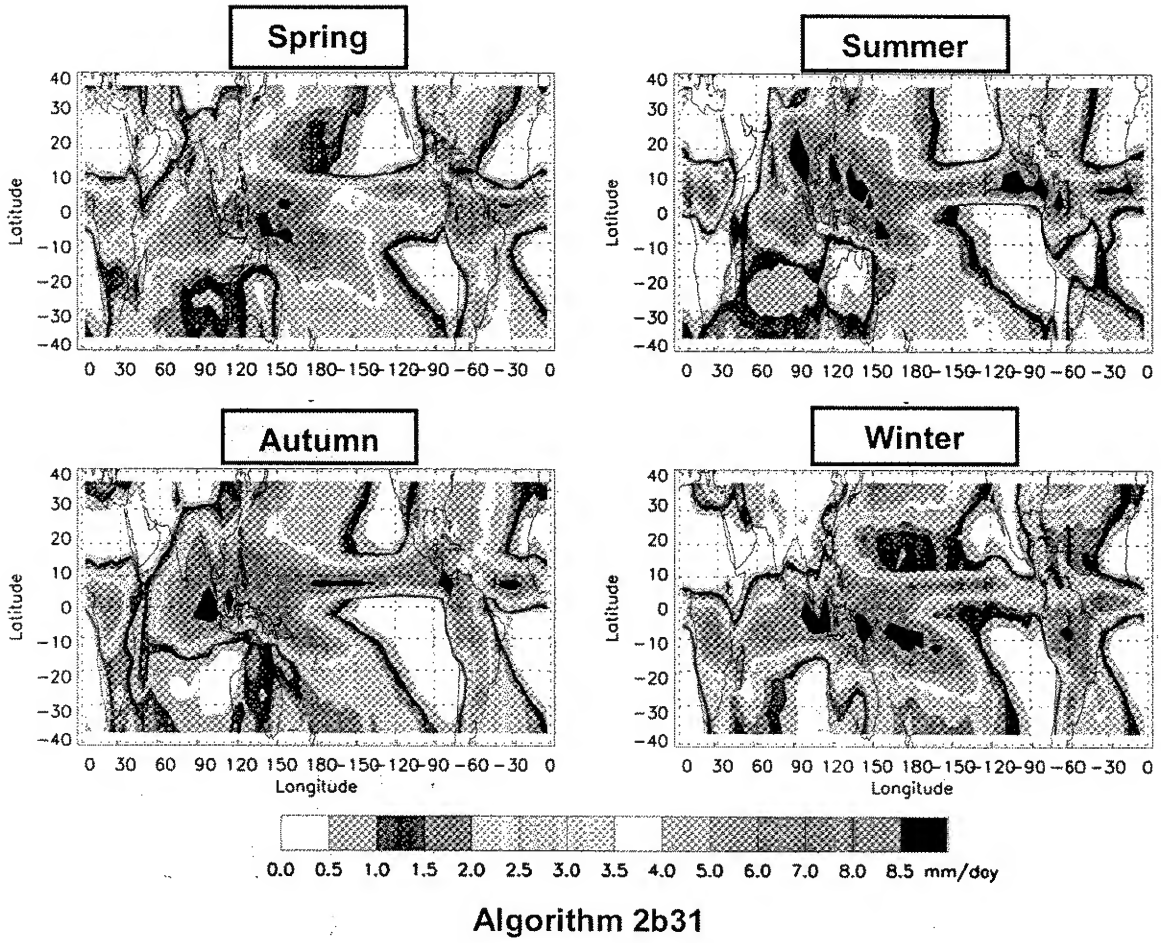

Figure 2: Horizontal distributions of 8-year mean seasonal rainrate (mm day^{-1}) from combined PR-TMI algorithm 2b31.

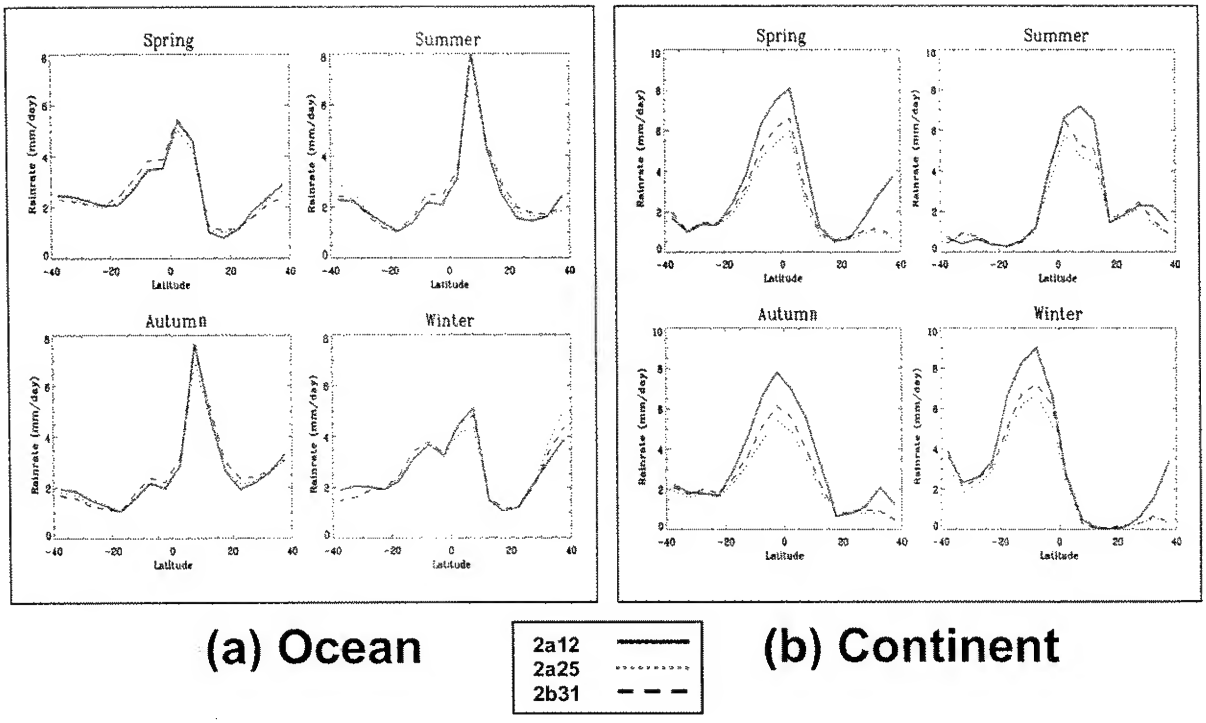

Figure 3: Zonal mean seasonal rainfall (mm day^{-1}) over (a) ocean and (b) continent for 8-years of rainrate measurements from algorithms 2a12, 2a25, and 2b31.

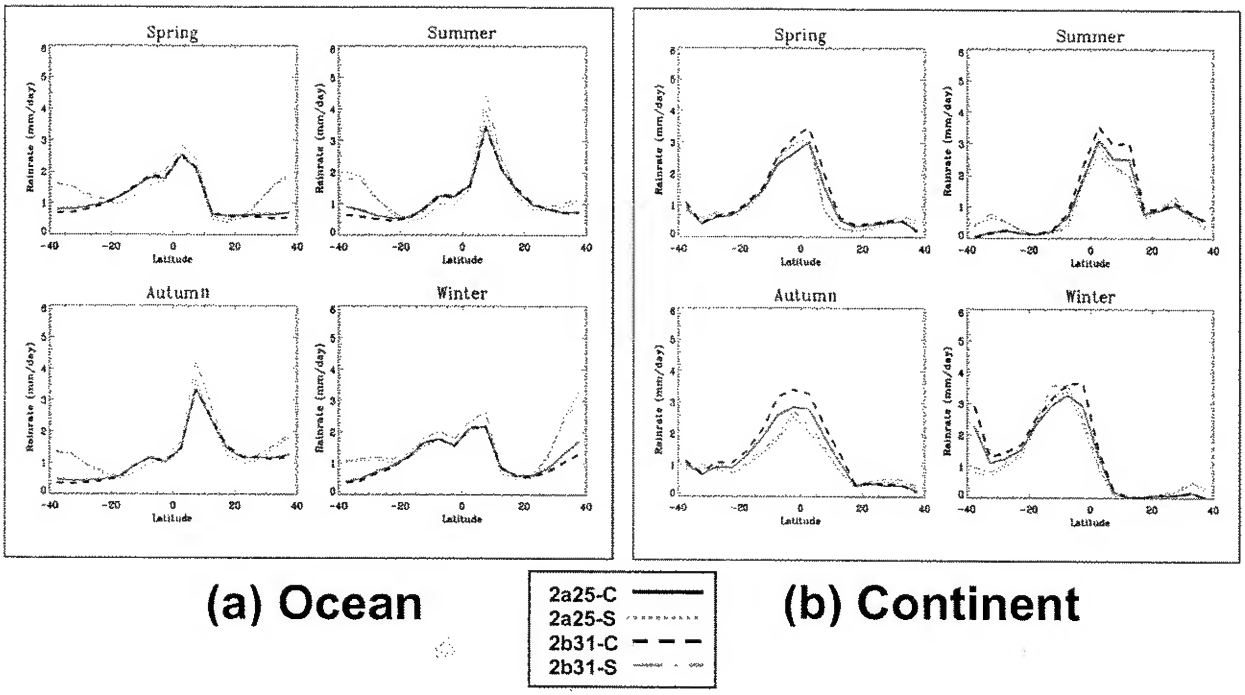

Figure 4: Zonal mean convective and stratiform rainfall (mm day^{-1}) over (a) ocean and (b) continent for 8-years of rainrate measurements from algorithms 2a25 and 2b31.

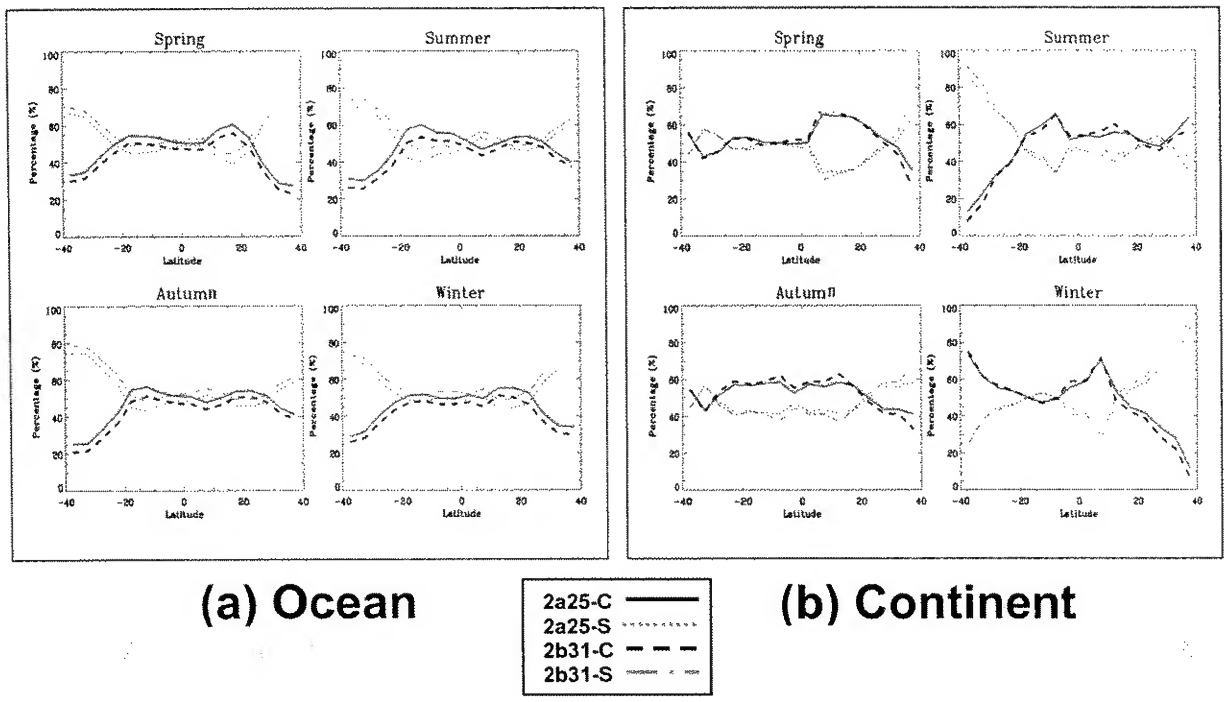

Figure 5: Zonal mean convective and stratiform seasonal rainfall contributions (%) for (a) ocean and (b) continent for 8-years of rainrate measurements from algorithms 2a25 and 2b31.

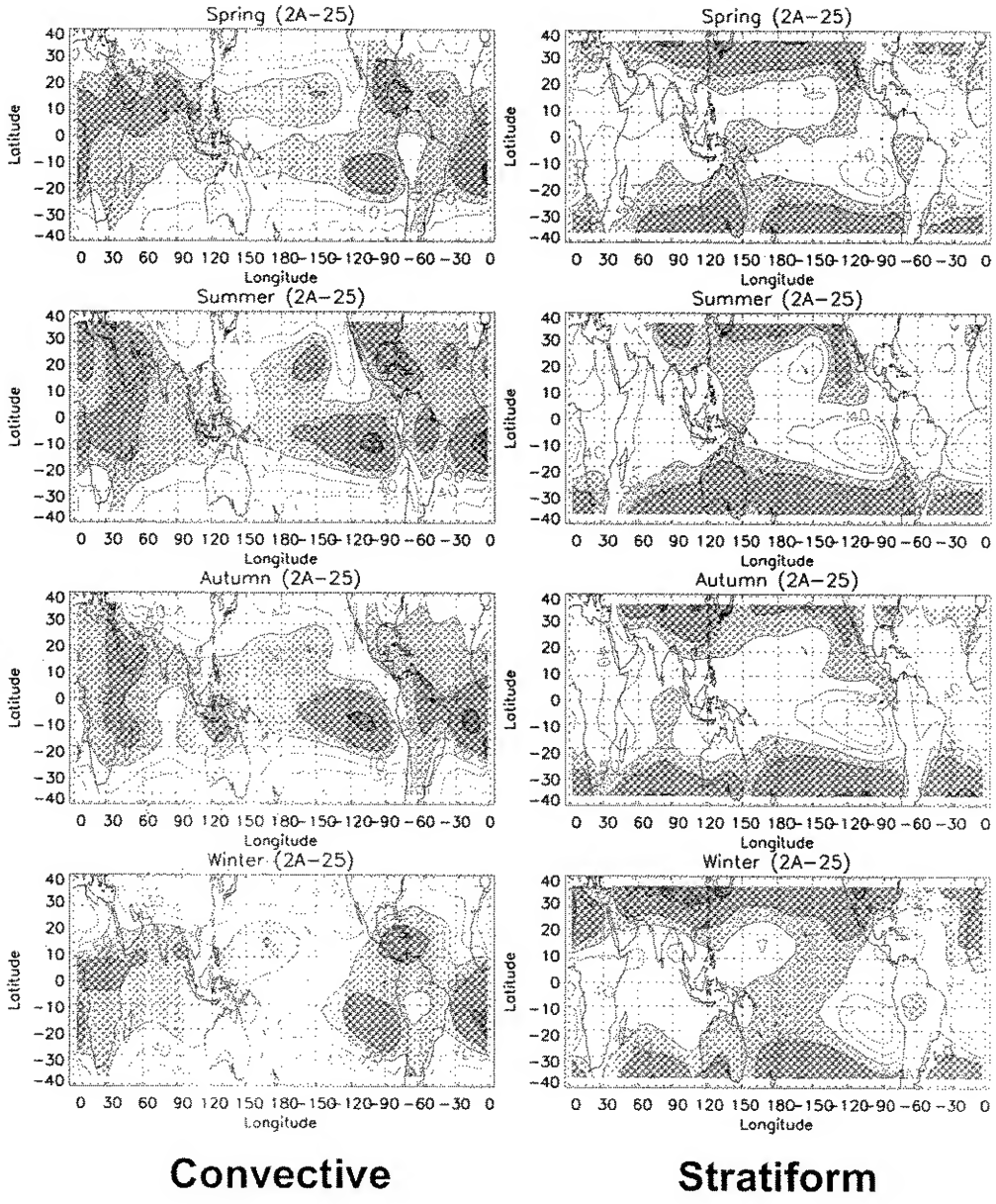

Figure 6: Horizontal distributions of mean seasonal convective and stratiform rainfall contributions (%) to total rainfall for 8-years of rainrate measurements from algorithm 2a25. Left panels show convective rainfall, while right panels show stratiform rainfall. Areas with values greater than 50%, 60%, and 80% are denoted with increasingly darker gray-shades.

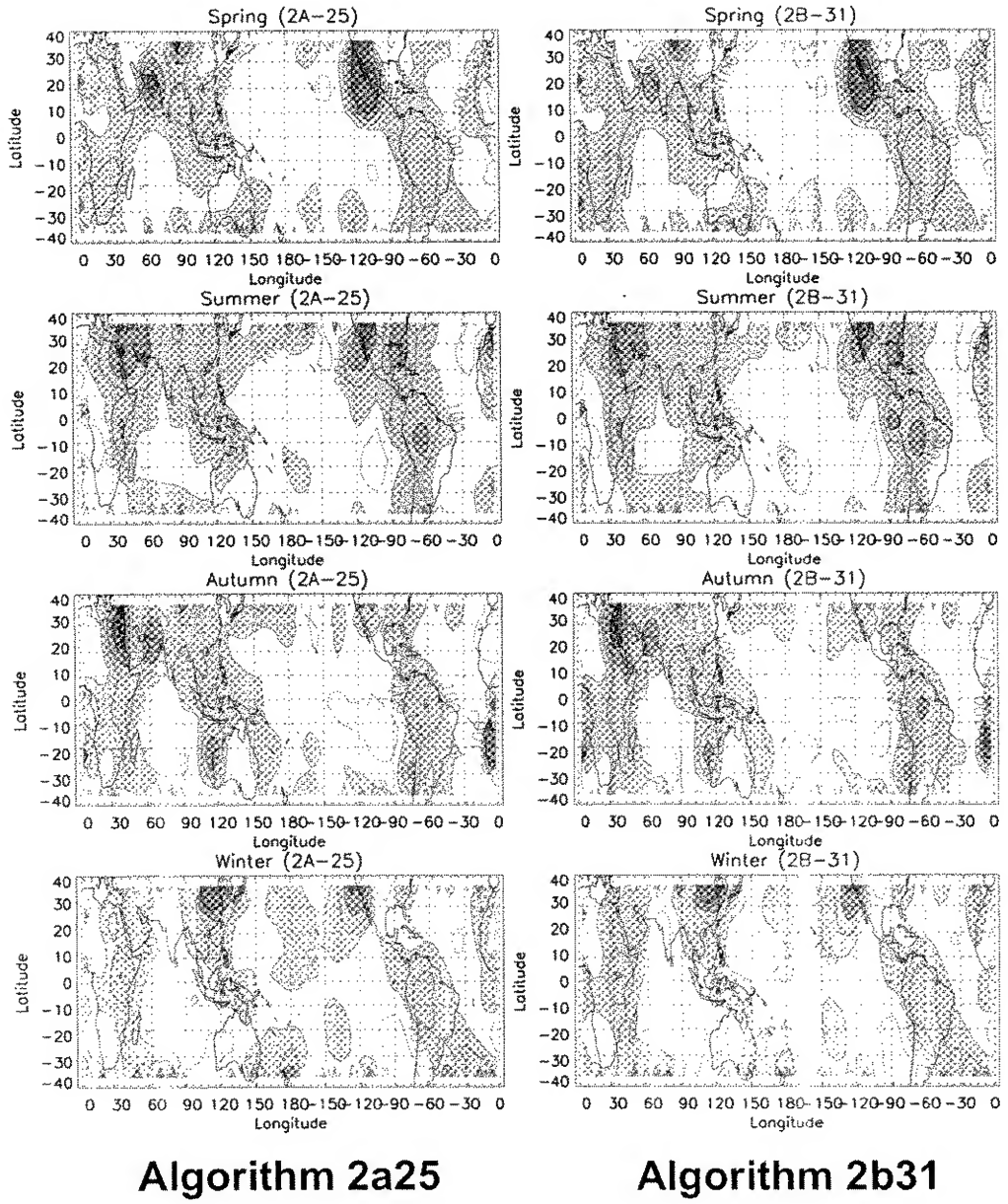

Figure 7: Horizontal distributions of ratio (%) between averaged daytime (numerator) and nighttime (denominator) seasonal rainfall for 8-years of rainrate measurements from algorithms 2a25 (left panels) and 2b31 (right panels), respectively. Areas with values greater than 100%, 125%, and 150% are denoted with increasingly darker gray-shades.

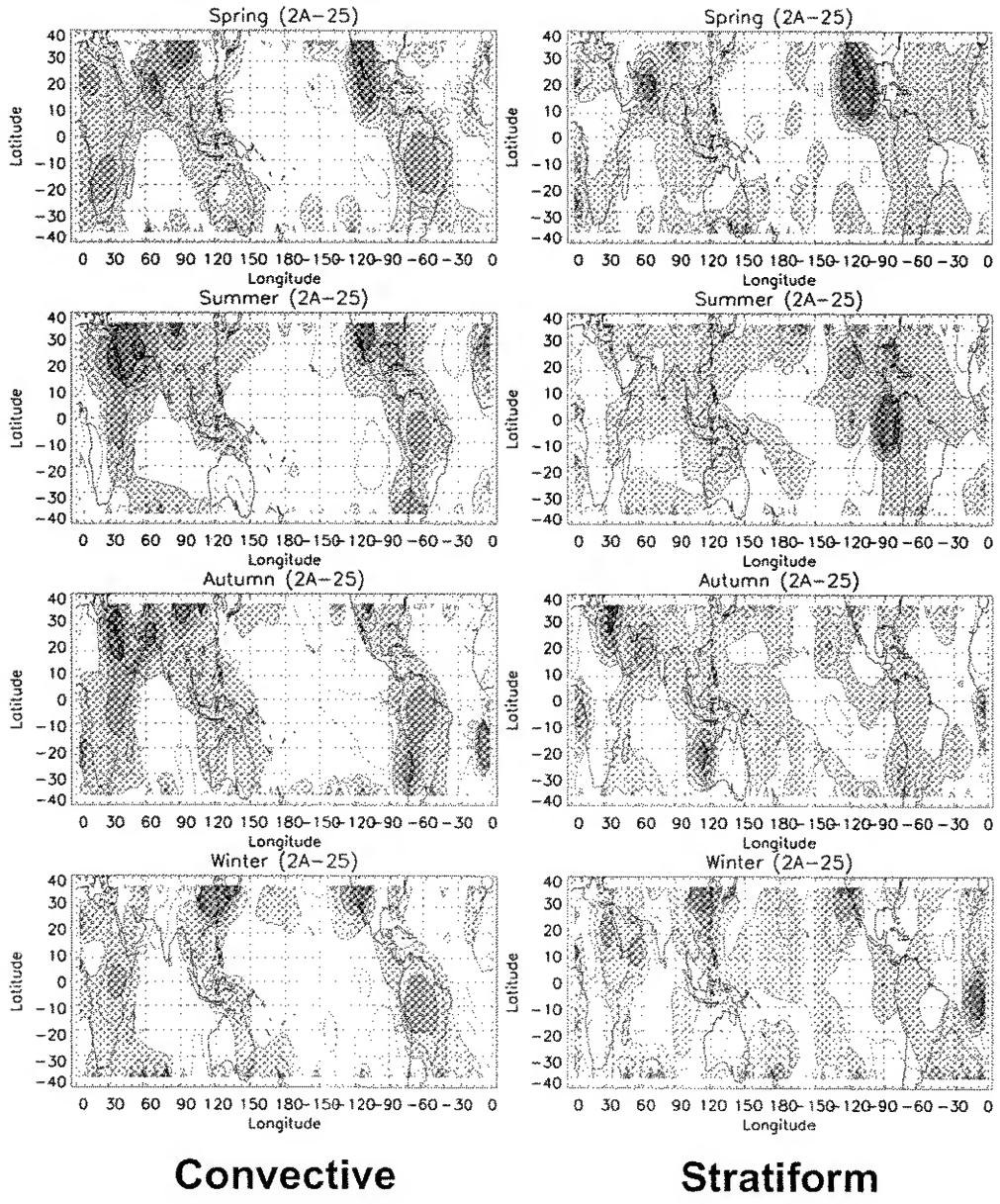

Figure 8: Horizontal distributions of ratio (%) between averaged daytime (numerator) and nighttime (denominator) seasonal convective and stratiform rainfall for 8-years of rainrate measurements from algorithm 2a25. Left panels show convective rainfall, while right panels show stratiform rainfall. Areas with values greater than 100%, 125%, and 150% are denoted with increasingly darker gray-shades.

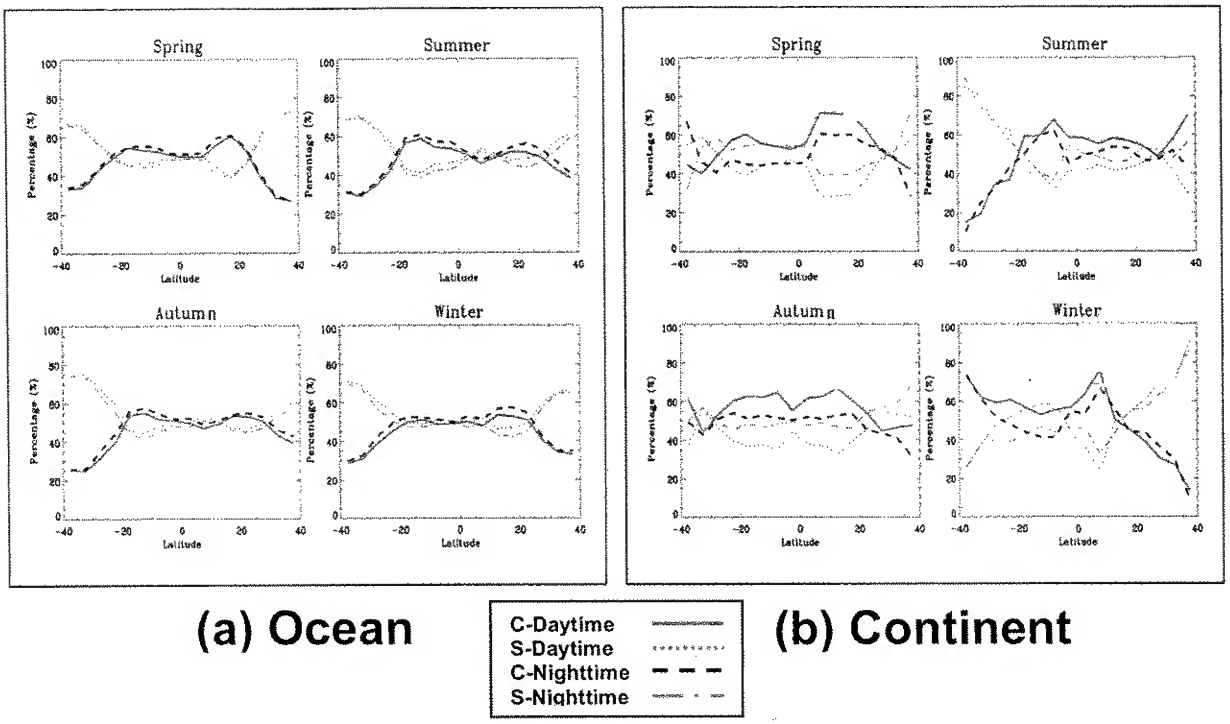

Figure 9: Zonal mean seasonal convective and stratiform rainfall contributions (%) during daytime (D) and nighttime (N) over (a) ocean and (b) continent for 8-years of rainrate measurements from algorithm 2a25.

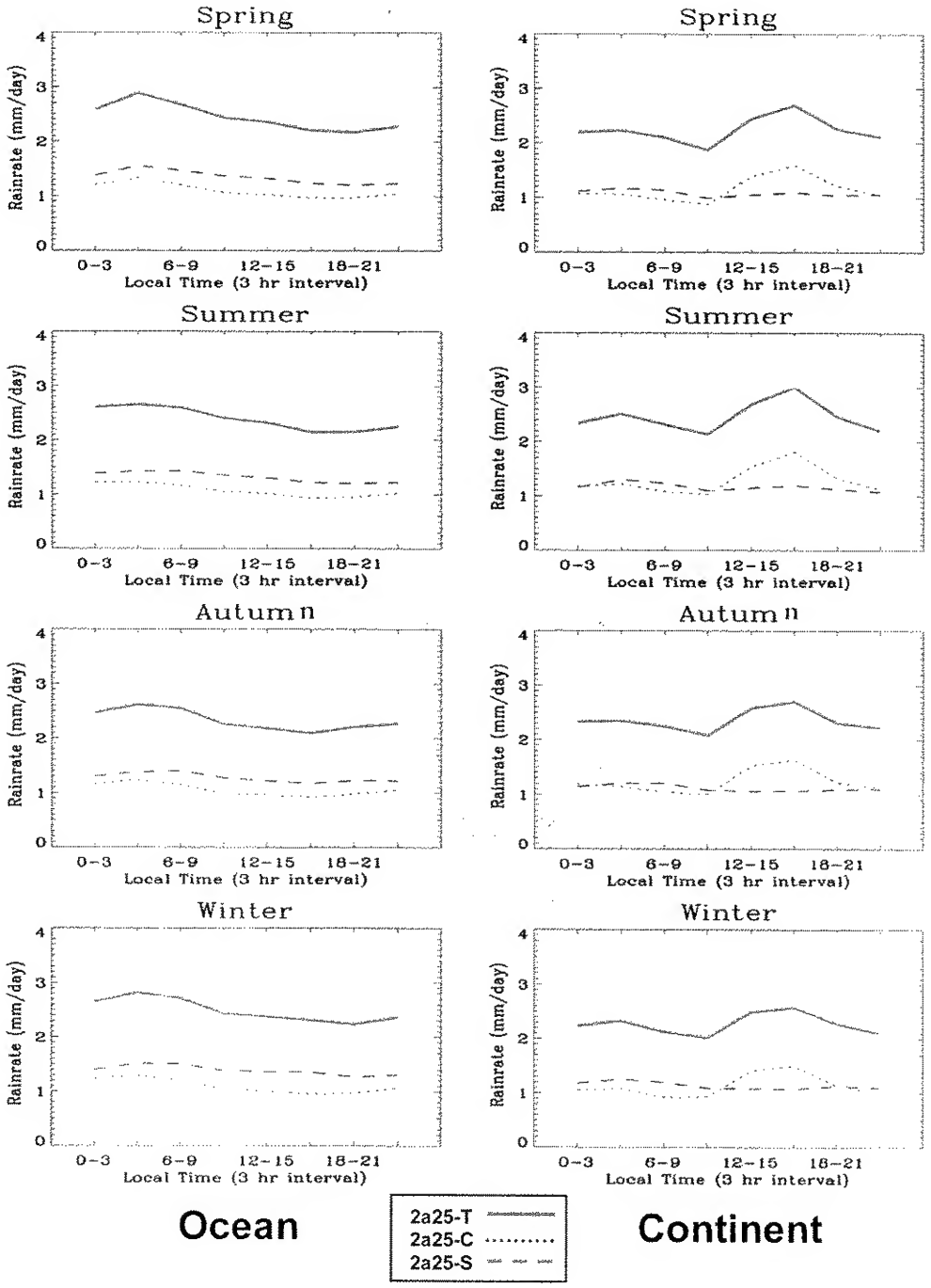

Figure 10: Diurnal cycle of mean seasonal rainfall (mm day^{-1}) partitioned into total (T), convective (C), and stratiform (S) categories over ocean (left panel) and continent (right panel) for 8-years of rainrate measurements from algorithm 2a25.

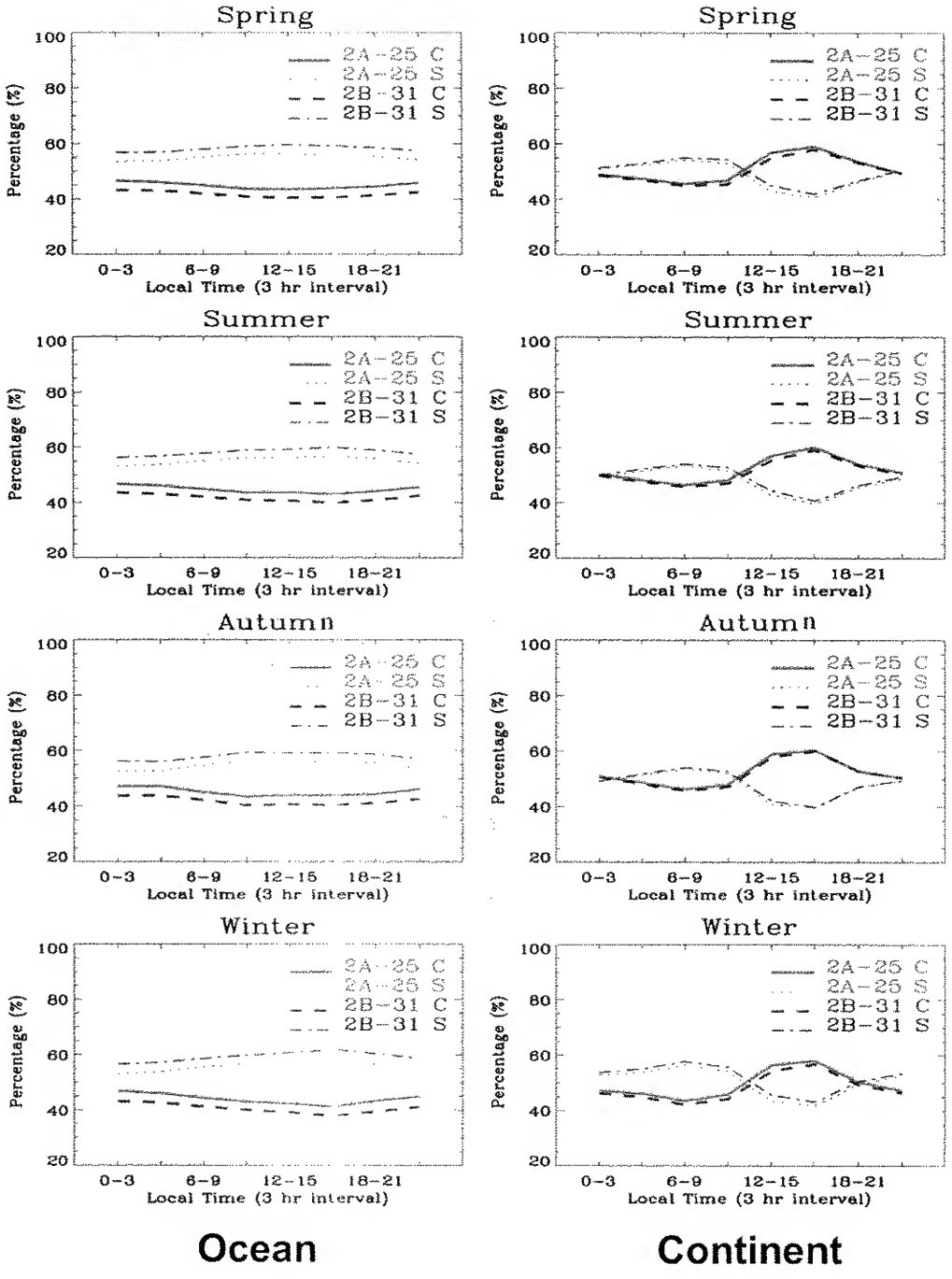

Figure 11: Diurnal cycle of mean seasonal convective and stratiform rainfall contributions (%) at each 3-hourly diurnal time interval over ocean (left panels) and continent (right panels) for 8-years of rainrate measurements from algorithms 2a25 and 2b31.

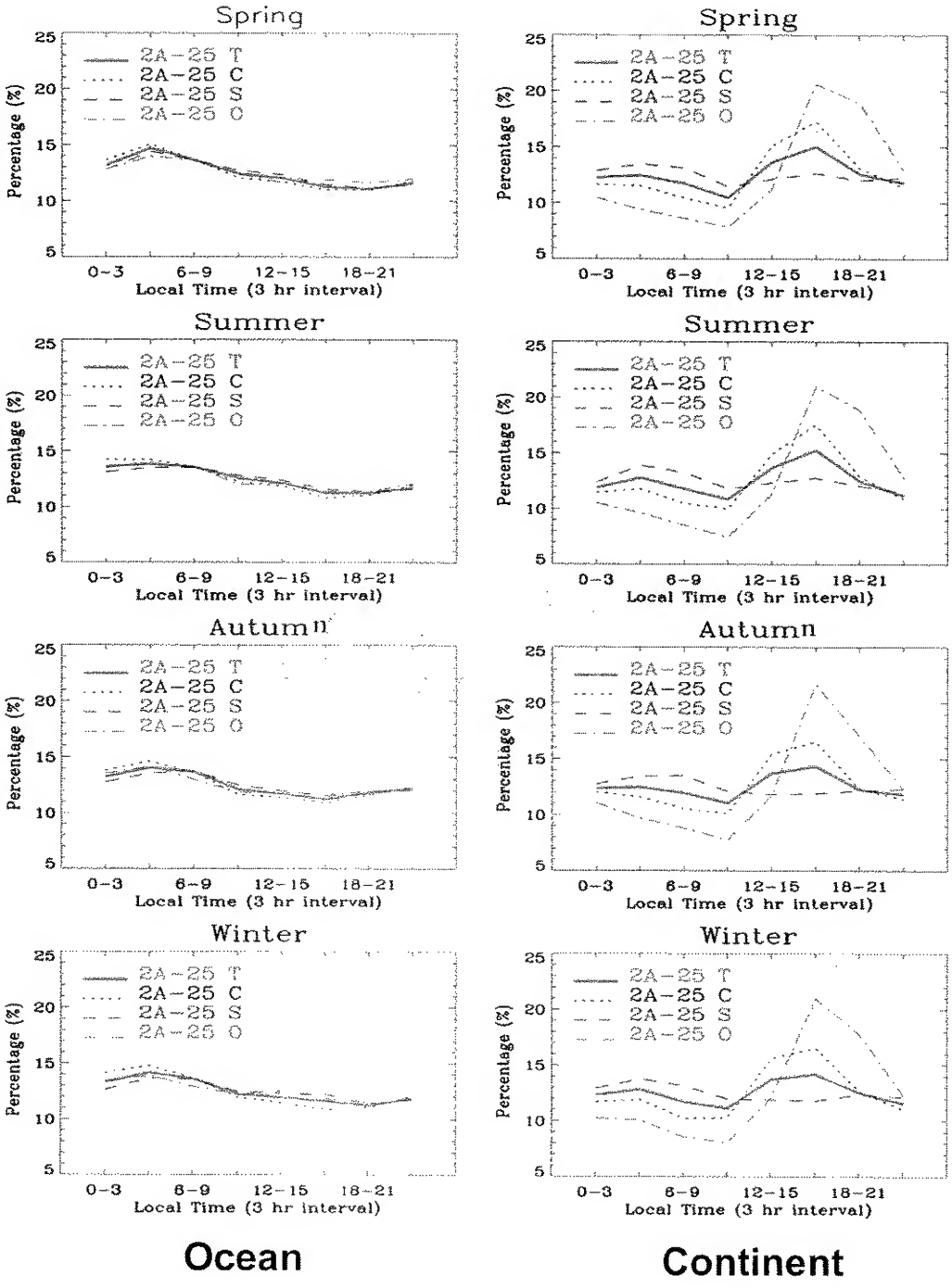

Figure 12: Diurnal cycle of relative contributions of rainfall in each 3-hourly diurnal time interval to total daily rainfall (%) for mean seasonal total (T), convective (C), stratiform (S), and "other" (O) rainfall over ocean (left panels) and continent (right panels) for 8-years of rainrate measurements from algorithm 2a25.

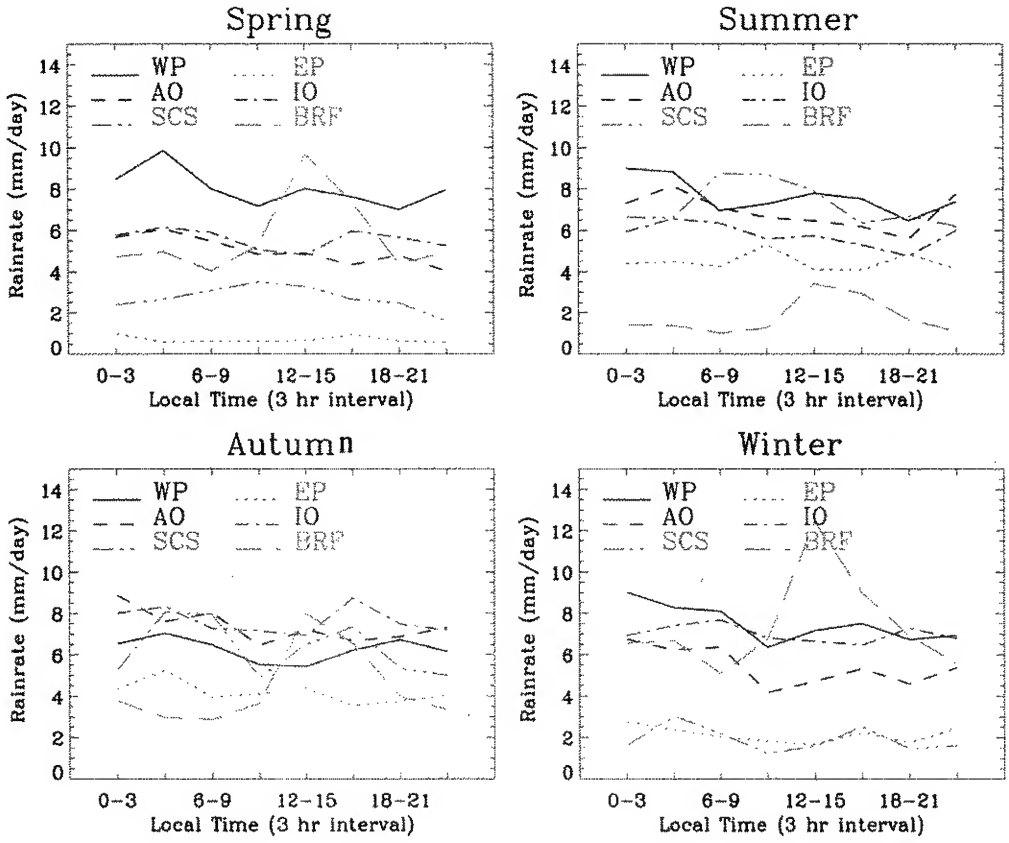

Figure 13: Diurnal variations of mean seasonal surface rainfall (mm day^{-1}) for 8-years of rainrate measurements from algorithm 2b31 over six regional domains: West Pacific (WP), East Pacific (EP), Atlantic Ocean (AO), Indian Ocean (IO), South China Sea (SCS), and Brazilian Rain Forest (BRF).

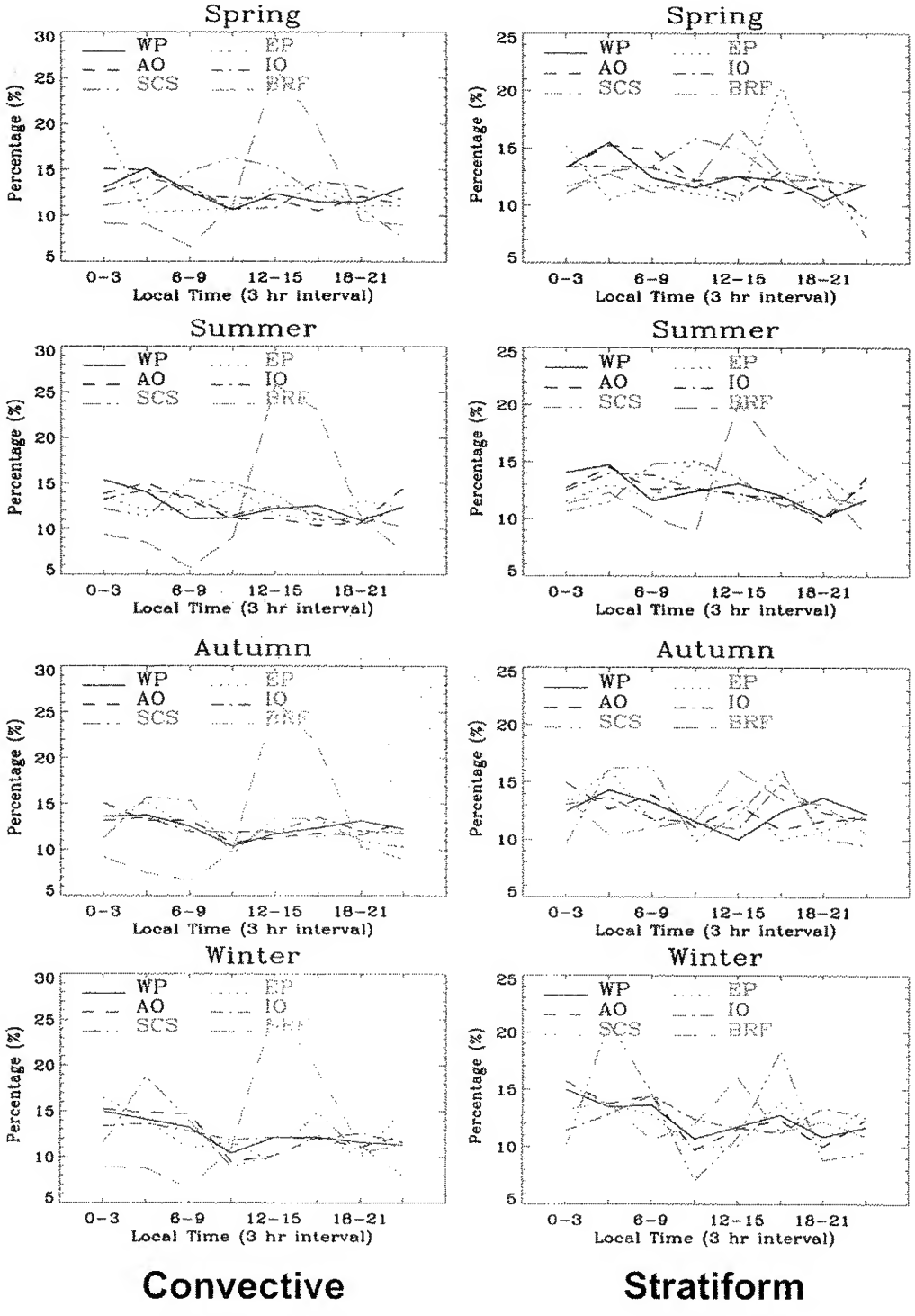

Figure 14: Diurnal variations of mean seasonal contributions (%) for convective (left panels) and stratiform (right panels) rainfall for 8-years of rainrate measurements from algorithm 2b31 over six regional domains identified in Fig. 13.

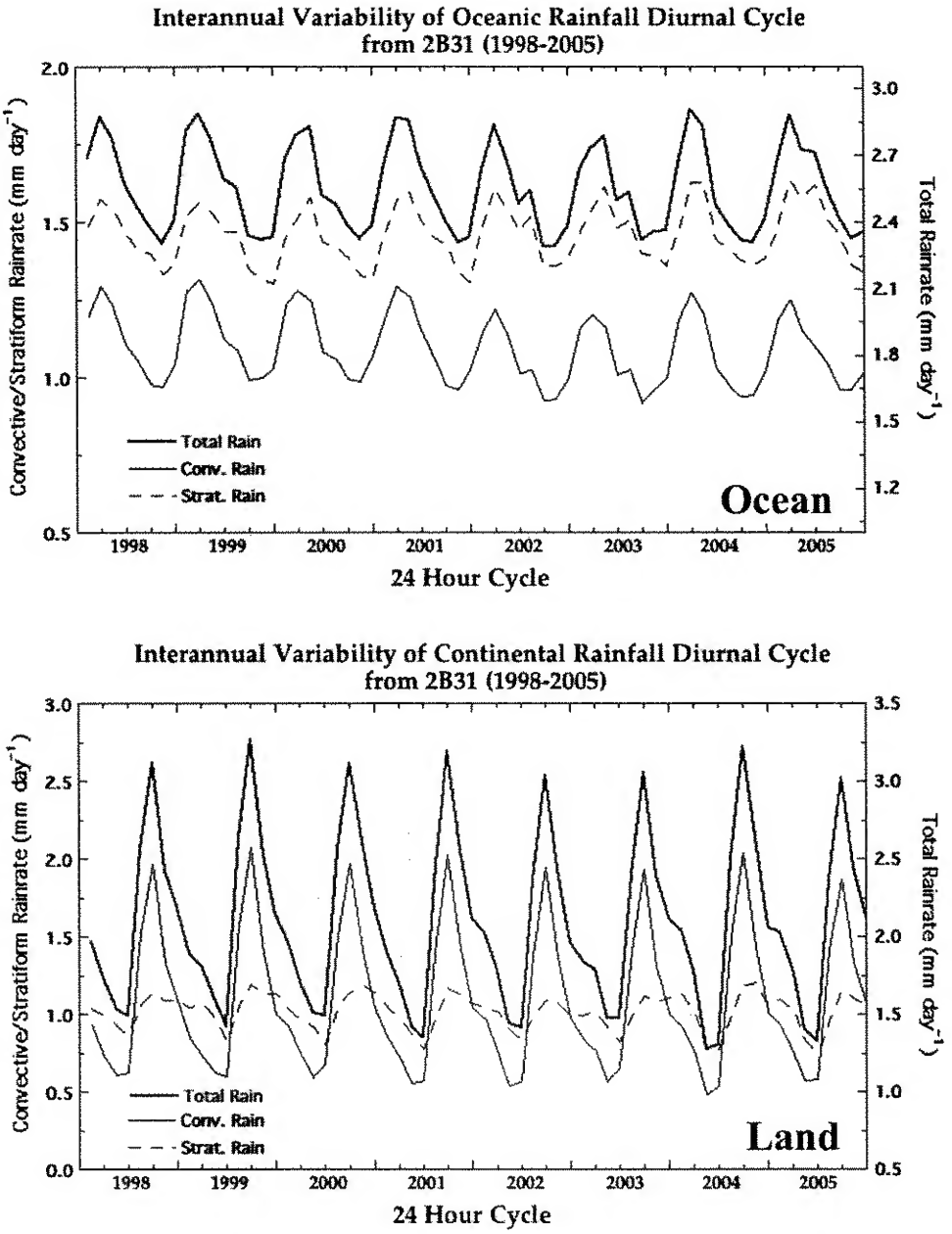

Figure 15: Interannual variability of mean oceanic and continental diurnal rainfall variability for total, convective, and stratiform rainfall categories for eight year TRMM 2b31. Each yearly segment on abscissa denotes 24-hour diurnal cycle from 00 to 24 MST. Left-hand (right) ordinates are assigned to convective and stratiform rainfall (total) variables (Unit: mm day^{-1}).